AD-A084 355 PENNSYLVANIA STATE UNIV UNIVERSITY PARK APPLIED RESE--ETC F/G 21/5
NATURE OF INLET TURBULENCE AND STRUT FLOW DISTURBANCES AND THEI--ETC(U)
FEB 80 R TRUNZO, B LAKSHMINARAYANA N00024-79-C-6043
UNCLASSIFIED ARL/PSU/TM-80-20 NL

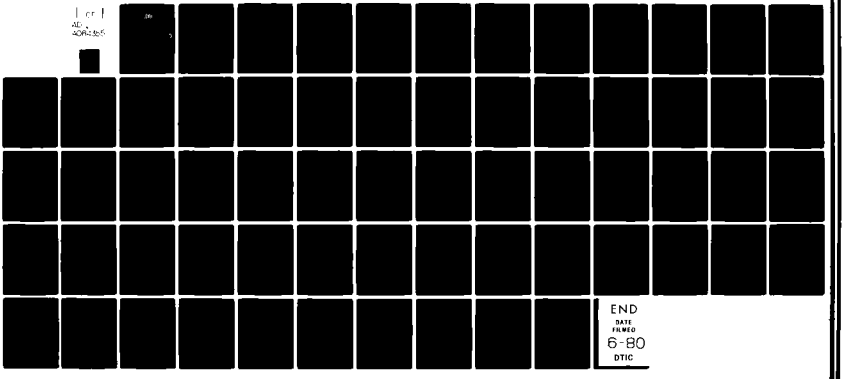

LEVEL II

NATURE OF INLET TURBULENCE AND STRUT FLOW DISTURBANCES AND THEIR EFFECT ON TURBOMACHINERY NOISE

R. Trunzo, B. Lakshminarayana and D. E. Thompson

Technical Memorandum
File No. TM 80-20
25 February 1980
Contract No. N00024-79-C-6043

Copy No. 53

The Pennsylvania State University
Institute for Science and Engineering
APPLIED RESEARCH LABORATORY
Post Office Box 30
State College, PA 16801

NAVY DEPARTMENT

NAVAL SEA SYSTEMS COMMAND

UNCLASSIFIED

SECURITY CLASSIFICATION OF THIS PAGE (When Data Entered)

REPORT DOCUMENTATION PAGE	READ INSTRUCTIONS BEFORE COMPLETING FORM
1. REPORT NUMBER: 80-20 ✓	2. GOVT ACCESSION NO.: AD-A084355
3. RECIPIENT'S CATALOG NUMBER	
4. TITLE (and Subtitle): NATURE OF INLET TURBULENCE AND STRUT FLOW DISTURBANCES AND THEIR EFFECT ON TURBOMACHINERY NOISE.	5. TYPE OF REPORT & PERIOD COVERED: Technical Memorandum
	6. PERFORMING ORG. REPORT NUMBER
7. AUTHOR(s): R. Trunzo, B. Lakshminarayana, D. E. Thompson	8. CONTRACT OR GRANT NUMBER(s): N00024-79-C-6043 ✓
9. PERFORMING ORGANIZATION NAME AND ADDRESS: Applied Research Laboratory ✓ P.O. Box 30 State College, PA 16801	10. PROGRAM ELEMENT, PROJECT, TASK AREA & WORK UNIT NUMBERS
11. CONTROLLING OFFICE NAME AND ADDRESS: David W. Taylor Naval Ship R&D Center Bethesda, MD 20084 (Code 1505)	12. REPORT DATE: 25 Feb 1980
	13. NUMBER OF PAGES
14. MONITORING AGENCY NAME & ADDRESS (if different from Controlling Office): Office of Naval Research 800 N. Quincy Street Arlington, VA 22217	15. SECURITY CLASS. (of this report): UNCLASSIFIED
	15a. DECLASSIFICATION/DOWNGRADING SCHEDULE

16. DISTRIBUTION STATEMENT (of this Report)

Approved for Public Release. Distribution Unlimited
Per NAVSEA - April 17, 1980.

17. DISTRIBUTION STATEMENT (of the abstract entered in Block 20, if different from Report)

14 ARL/PSU/TM-80-20

18. SUPPLEMENTARY NOTES

Sponsored by the Naval Sea Systems Command, General Hydromechanics Research Program administered by David W. Taylor Naval Ship Research and Development Center, Code 1505, Bethesda, MD 20084

19. KEY WORDS (Continue on reverse side if necessary and identify by block number)

turbomachinery, rotor, sound, spectra, aerodynamic, measurements, correlation

20. ABSTRACT (Continue on reverse side if necessary and identify by block number)

Results of an investigation in which turbomachinery rotor sound spectra were correlated with aerodynamic measurements of the inlet turbulence, strut wake, and vortex flow strengths are reported. Aerodynamic measurements included mean velocity profiles, turbulence intensity, and axial length scales. Inlet turbulence data indicate that the major effect of flow contraction appears to be the elongation of turbulent eddies from 20 cm to 200 cm. Eddies of this size dominate the blade passing frequency (BPF) tones. Decreasing eddy size

DD FORM 1 JAN 73 1473 EDITION OF 1 NOV 65 IS OBSOLETE

391007

UNCLASSIFIED

SECURITY CLASSIFICATION OF THIS PAGE (When Data Entered)

20. by use of a grid revealed vortex flow strength to be the second major sound source. A doubling of vortex flow strength produced a 6 dB increase in the SPL of the first BPF. The sound pressure level showed less than a 2 dB change with doubling of wake turbulence intensity or velocity defect. A discussion of the relative importance of various sources of noise due to flow distribution at the inlet is given. This report will be submitted to the Journal of Sound and Vibration for publication.

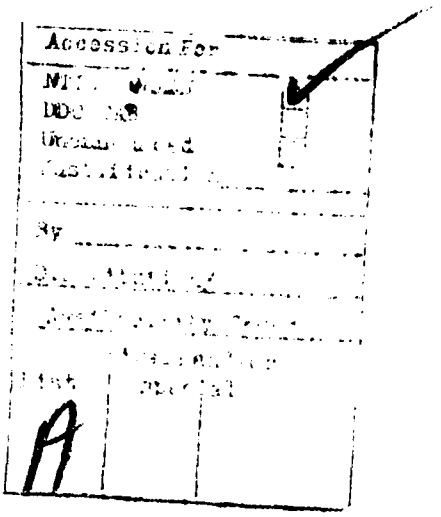

Subject: Nature of Inlet Turbulence and Strut Flow Disturbances and Their Effect on Turbomachinery Noise

References: See page 22.

Abstract: Results of an investigation in which turbomachinery rotor sound spectra were correlated with aerodynamic measurements of the inlet turbulence, strut wake, and vortex flow strengths are reported. Aerodynamic measurements included mean velocity profiles, turbulence intensity, and axial length scales. Inlet turbulence data indicate that the major effect of flow contraction appears to be the elongation of turbulent eddies from 20 cm to 200 cm. Eddies of this size dominate the blade passing frequency (BPF) tones. Decreasing eddy size by use of a grid revealed vortex flow strength to be the second major sound source. A doubling of vortex flow strength produced a 6 dB increase in the SPL of the first BPF. The sound pressure level showed less than a 2 dB change with doubling of wake turbulence intensity or velocity defect. A discussion of the relative importance of various souces of noise due to flow distribution at the inlet is given. This report will be submitted to the Journal of Sound and Vibration for publication.

Acknowledgments: This work was performed under the Naval Sea Systems Command General Hydromechanics Research Program Subproject SR 023-01-01, administered by the David W. Taylor Naval Ship Research and Development Center. Authors wish to thank Dr. Homicz for providing them with a copy of the computer program based on Reference 12 and Mr. J. H. Rishell for providing help in data acquisition.

TABLE OF CONTENTS

NOMENCLATURE

C_D	Drag coefficient of the blade
c	Blade chord
d	Diameter of the duct
L_W	Wake width based on semidepth nondimensionalized by rotor blade spacing
r, r_t	Local and tip radius of the blade
s/c	Space to chord ratio
U_x, U_{x_o}	Axial component of velocity in the freestream
U_c	Velocity at mid radius
U_{xr}	$\sqrt{U_x^2 + U_r^2}$
U_r	Radial velocity
u, v, w	Turbulent velocity in axial, tangential and radial directions respectively
$\sqrt{\overline{u^2}}/U_x$	Axial component of turbulence intensity
$\sqrt{\overline{v^2}}/U_x$	Tangential component of turbulence intensity
q^2	$(u^2 + w^2)$
Y	Strut wake transverse distance normalized by the local rotor blade spacing (Y = 0 at the wake center)
z	Distance between hot wire probe and strut trailing edge (Figure 2) for aerodynamic measurements, distance between rotor leading edge and strut trailing edge for acoustic measurements
Z	z/c
Λ	Velocity defect in the wake $(1 - U_{xr}/U_{xo})$
ξ	Strength of the vorticity
θ	Arc location (Figure 49)
ϵ	Blade turning angle
ϕ	Flow coefficient (axial velocity divided by the blade speed)
δ	Strut boundary layer thickness

LIST OF TABLES

LIST OF FIGURES

INTRODUCTION

The generation of sound by low speed turbomachinery rotors is known to be a function of the blade geometry as well as upstream flow characteristics. The latter category would include the inlet turbulence, centerbody and annulus wall boundary layer turbulence, mean flow distortions and turbulence caused by vortices and wakes of upstream struts. The broadband sound arises due to random velocity fluctuations in wall and blade boundary layers as well as the free stream. The pure tone noise arises from the elongated turbulent eddies present in the free stream, as well as the mean velocity defect in wakes and boundary layers. An experimental investigation in which the effect of long eddies present in the free stream and the wall boundary layers was systematically studied is discussed in References [1]* and [2]. The effect of disturbances (both random and periodic) caused by upstream struts has not been studied systematically. The upstream struts generate noise through interaction of the rotor with wakes shed at all spanwise locations and with the vorticity generated near the intersection of the centerbody with the struts. Furthermore, the turbulence in the wake and vortex flow regions generate both broadband and pure tone noise. The objective of this paper is to study these effects as sources of noise and to ascertain their relative importance in the overall noise generation.

The investigation reported here can be broadly classified into two phases. During the first phase, effort was directed towards an understanding of the eddy elongation process as it travels from upstream of the inlet to a position upstream of the rotor. The second phase of the investigation consisted of the study of the strut generated noise. This study was carried out with four upstream struts, operated at various strut-to-rotor spacings. The flow field, as well as the noise levels, were measured. The correlation of the mean velocity and turbulence data (in the wake, as well as end wall regions) with the far field noise levels provide some important information on the effect of various sources of strut disturbance on noise generation.

*Numbers in brackets refer to references at the end of the paper.

EXPERIMENTAL FACILITY AND PROGRAM

Aeroacoustic Facility

An aeroacoustic facility was used for this investigation. The facility, shown in Figure 1, consists of four main components: an anechoic chamber, a 17.53 cm diameter test rotor, an acoustic diffuser and baffle chamber, and a Joy axial flow fan. The test medium is air. A hot wire probe positioning mechanism which did not alter the flow was removed for all acoustic measurements. A detailed description of the facility as well as the rotor is given by Robbins and Lakshminarayana [1].

Interior dimensions of the anechoic chamber were 3.35 x 3.66 x 2.44 m. The walls, floor, and ceiling were constructed of Ovens-Corning Type 705 industrial fiberglass, 15.24 cm thick. The rotor inlet was centered in one wall of the chamber with the inlet lip 38.0 cm from that wall. An inlet hole 1.0 m in diameter located directly opposite the rotor inlet admitted air into the chamber. A 5.04 cm thick fiberglass baffle upstream of the hole prevented noise from entering the chamber. Calibration of the anechoic chamber showed that the measured data is in good agreement with the inverse square law from 1 to 20 kHz. The ambient noise level was measured to be 20 dB below the rotor noise spectrum. These results indicated the chamber to be anechoic for the frequency range of interest in this investigation and to have acceptable ambient noise levels.

A 17-bladed rotor was used in conjunction with four symmetric struts for all tests. The rotor blade chord was nearly constant from the centerbody to tip at 4.06 cm. The rotor blade spacing at mid span was 2.43 cm. The stagger angle varied from 0.31 radians at the root to 0.81 radians at the tip. The centerbody-to-tip ratio of the rotor was 0.48. The struts used had NACA 0021 symmetric profiles with no twist, a zero incidence and chords of 12.7 cm. The rotor was operated at 5440 rpm with an axial velocity of 39.0 m/sec. This resulted in a flow coefficient of $\phi = 0.75$. The aerodynamic performance of the rotor is documented by Moiseev, et al. [2].

Aerodynamic Configurations and Measurements

Strut wake width, velocity defect and turbulence were varied by changing the rotor-to-strut spacing as illustrated in Figure 2. Three spacings, nondimensionalized with respect to the strut chord, were investigated; $Z = 0.18$, 0.9, and 1.8 where Z = nondimensional distance between the probe and the trailing edge of the strut. The effect of vortices generated at the intersection of a strut with the inner wall was also investigated. Since the strength as well as size of these vortices are strongly related to the boundary layer thickness, as illustrated by Barber [3], the centerbody length was shortened from 47.63 cm to 26.35 cm to provide two different boundary layer thicknesses.

It should be remarked here that all the aerodynamic measurements were carried out with the configuration just described in Figure 2, keeping the rotor and the probe location fixed and moving the strut. For noise measurements, the velocity survey ring shown in Figure 2 was removed and the struts moved closer to the rotor such that the distance between the rotor leading edge and the strut trailing edge nondimensionalized by the strut chord, was 0.18, 0.9 and 1.8. Hence, the aerodynamic measurements reported here correspond to the flow field that would exist at the leading edge of the rotor, neglecting the upstream influence of the rotor on the flow field. This method was adopted because of the difficulties in carrying out measurements close to the rotor leading edge.

The final parameter investigated was the effect of inlet turbulence on rotor noise in the absence of struts. Turbulence levels and length scales were measured at axial stations 6.71 cm and 31.39 cm upstream of the rotor. Measurements were also conducted at stations 10.31 cm and 17.6 cm upstream of the inlet along a circular arc, as shown in Figure 3. The effect of a grid altered turbulence was also studied. The grid, placed in the annulus 59.69 cm upstream of the rotor Figure 3, has a mesh size of 2.86 cm and a rod diameter of 0.556 cm. For all experiments, the free stream velocity and flow coefficient were held constant.

An x-array hotwire probe was used to obtain axial and tangential components of mean velocity and turbulence. Probes were calibrated accounting for temperature variations. The calibration was repeated before and after each test to account for the variation in wire resistance due to wire aging. The flow was surveyed 45° to either side of the strut chordline at two radii, 54% and 75% of the rotor tip radius. Surveys of 360° were also conducted at these radii plus at a radius of 95% of the tip radius for the purpose of Fourier analyzing the rotor inflow.

In conjunction with the standard hotwire anemometry network, a correlation function computer was used. The autocorrelation of the axial component of velocity (u) was recorded by using an x-y plotter. An integral time scale was derived from this curve by using the following equation:

$$\int_0^\infty \rho_{uu}(\tau)d\tau = T$$

where $\rho_{uu}(\tau) = \overline{u(x, y, \theta, t)\, u(x, y, \theta, t + \tau)}/u^2$ and x, r, θ are the axial, radial and tangential directions, respectively. By assuming that turbulent eddies were convected with the flow, multiplication of the time scale by the local axial velocity gave the axial length scale (L_x).

Acoustic Measurements

The acoustic measurements were carried out with the struts placed at 0.18, 0.9 and 1.8 chordlengths upstream of the rotor leading edge, as described earlier. In Figure 2, "z" now corresponds to the distance between the leading edge of the rotor and the trailing edge of the struts.

Measurements of the far-field noise spectra were carried out with a 0.64 cm diameter B&K condensor microphone. Noise spectra were obtained by analyzing the microphone signal with a General Radio wave analyzer and recording the output signal with an x-y plotter. The relative dB levels of the rotor blade passing frequency and harmonics were also measured by time averaging the mean square output of the wave analyzer (at the frequency of interest) over a 60-second time period. The bandwidth of the analyzer was 10 Hz. The microphone was located 76.2 cm in front of the inlet, Figures 2 and 3, along the annulus centerline. All hotwire probes were removed during noise measurements.

Due to the length of the inlet annulus, some concern was expressed for its effect on the rotor noise propagation. Results indicated the first mode of the annulus was at 4 kHz, which corresponds to a wavelength twice the annulus size. This is well above the first and second blade passing frequency (BPF). Thus, the spectra are <u>not</u> corrected for the annulus response.

Spectra were obtained for all the configurations mentioned in the previous section. Table I summarizes the parameters varied and the measured sound pressure levels (SPL) of the first, second, and third blade passing harmonics. The rotor was operated at 5,440 rpm, at a flow coefficient of $\phi = 0.75$ and an axial velocity of 39 m/sec for all tests.

INLET CONTRACTION EFFECTS ON ENTRY TURBULENCE

Inlet Flow Characteristics

The results of the mean velocity profile measurements are shown in Figure 4. In Figure 4a, the axial velocities are nondimensionalized with respect to the axial velocity at the annulus centerline ($\theta = 90°$). The axial centerline velocities at stations 3 and 4, see Figure 3, were 4.04 m/sec and 1.79 m/sec, respectively. The increase in the axial velocity ratio as the probe moved from $\theta = 90°$ to $\theta = 0°$ was the result of the decrease in effective cross sectional area.

The axial mean velocity profiles at stations 1 and 2 are shown on Figure 4b. Free stream velocities at these stations were 35.8 m/sec at station 1 and 28.4 m/sec at station 2. The larger velocity gradient at the wall for station 1, compared to station 2, was the result of boundary layer growth. The velocity profile developed on the stationary 47.63 cm long centerbody, originally measured by Moiseev et al. [2] and repeated in this investigation, shows clearly the thick boundary layer on the inner and outer walls.

The variation of the axial ($\sqrt{\overline{u^2}}/U_x$) and tangential ($\sqrt{\overline{v^2}}/U_x$) components of turbulence are shown in Figures 5 and 6. Upstream of the inlet, the turbulence was found to be weekly nonisotopic. This degree of nonisotropy was maintained from the inlet to the rotor with the tangential intensity being slightly higher than the axial component. The axial and tangential intensities upstream of the inlet and at the rotor differ by approximately 40%.

The axial and tangential intensities at stations 1 and 2, Figure 3, are shown in Figure 6a and 6b, respectively. Also shown is the intensity profile with a long centerbody. It is evident that axial and tangential intensities remain nearly constant in the free stream from stations 4 through 1. The intensities are substantially higher in the annulus wall and centerbody wall boundary layers.

To verify the trends exhibited by the turbulence intensity components, the measurements were compared to a theory on the effect of contraction on isotropic turbulence by Ribner and Tucker [4]. The behavior of the turbulent velocities $\overline{u^2}$ and $\overline{v^2}$ in an axisymmetric contraction were determined by the following equations

$$\frac{\overline{u_B^2}}{\overline{u_A^2}} = \frac{3}{4\ell_1^2}\left[\frac{-1}{1-\epsilon} + \frac{2-\epsilon}{(1-\epsilon)^{3/2}}\tanh^{-1}\sqrt{1-\epsilon}\right], \qquad (2)$$

$$\frac{\overline{v_B^2}}{\overline{v_A^2}} = \frac{3}{8\ell_2^2}\left[\frac{2-\epsilon}{1-\epsilon} - \frac{\epsilon^2}{(1-\epsilon)^{3/2}}\tanh^{-1}\sqrt{1-\epsilon}\right]. \qquad (3)$$

where subscripts A and B refer to stations upstream of and downstream of the contraction, respectively, $\epsilon = A_B^2/A_1^2$, ℓ_1 = ratio of velocity at station B to that at station A, and ℓ_2 = stream breadth at station B divided by its value at station A. Comparison of measurements with the theory

are shown in Figure 7. The experimental data agree well with predictions from Equations 2 and 3.

The effect on turbulence intensity of a grid placed at the inlet is illustrated in Figure 8. The axial and tangential turbulence intensities are plotted for stations 1 and 2. Comparison of the grid and no grid cases indicates that, in the vicinity of the grid, axial and tangential intensities are increased by a factor of nearly 6 and 3, respectively. A second effect of the grid is to reduce the non-isotropy of the flow. Even though the intensities are increased when the grid is inserted, the length scales were decreased as explained below.

The measured axial length scales at various axial and radial locations are tabulated in Table II. It is evident that the scales upstream of the inlet are of the same order of magnitude as the annulus diameter. The length scale increases drastically as the flow goes through the contraction from station 4 to 1. The length scale at the center of the annulus increases ten-fold from station 4 to 1. In addition, there is a small variation in length scale across the annulus. Based on the measurements reported in this paper, one can conceptually imagine the stretching of the eddies as shown in Figure 9.

Hanson [8] was one of the first to identify these long eddies as a source of noise. Since each of these eddies are chopped several times over as it passes through the rotor, partially coherent noise is generated. This contributes to and/or increases the spectral peaks. It is somewhat surprising that the eddies are long (of the order of an annulus diameter) even before they enter the inlet.

Correlation of Inflow Turbulence Data

A comparison of inflow data reported here with data obtained by other investigators is shown in Table III. Each investigation is classified on the basis of where measurements were made, as follows: (1) measurements upstream of the inlet, (2) measurements forward of the centerbody but downstream of the inlet, and (3) measurements in the annulus region. Important parameters listed in Table III are the type of facility used, source of turbulence, annulus outer diameter (d), height of annulus centerline above the floor, type and location of probe used, number of rotor blades (N) and the centerbody-to-tip ratio (r_h/r_t). Also listed for each investigation are the free stream values of both axial and tangential turbulence intensity, axial length scale (L_x), free stream velocity (U_x), flow coefficient (ϕ), and the ratio of tip to axial Mach numbers (M_t/M_a).

It should be remarked here that the research reported in this paper is the only available investigation aimed at the study of the development of turbulent eddies as they pass from upstream of an inlet to the rotor leading edge, as is evident from Table III.

In the region upstream of the centerbody and downstream of the inlet Figure 3, flow contraction results in a slight decrease in the magnitude of both the components of turbulence. A greater decrease in the tangential intensity occurs as the turbulent eddy is stretched.

Comparison of this data with those of Bekofske, et al, [5] shows a discrepancy in the relative magnitudes of the turbulence intensities. In the two types of inflow turbulence measured by Bekofske, et al, [5], the axial intensities were found to be greater than the tangential intensities. This result can be explained by analyzing the generation of the inflow turbulence. Inflow turbulence in the first part of the study by Bekofske et al [5] was generated by drawing air through the porous walls of the anechoic chamber. Turbulence intensity levels were measured at 1.7% and 1.2% for the axial and tangential components. The second inflow turbulence investigation was performed with all air ducts to the walls closed. Air was admitted only through doors in the wall opposite the fan inlet. The result was an increase in the tangential intensity from 1.2% to 1.6% with no increase occurring in the axial intensity. When this is taken into consideration with the longer axial length scales, it is evident that a larger scale of turbulence is being ingested by the inlet. Thus, a trend is exhibited that with larger room eddies present, a higher tangential intensity is encountered. Based on this idea, a difference in the size of room turbulence could account for the discrepancy between Bekofske's measurements and those of this investigation.

The largest discrepancy between components of turbulence intensity was that measured by Shaw, et al [6]. In their investigation, the tangential turbulence intensity was ten times larger than the axial intensity. Shaw [7] indicated that a control door on the wind tunnel might have been open which may account for high tangential intensities being measured.

The final class of measurements are those taken in the annular region. Measurements from this investigation are compared to data from studies by Hanson [8], Robbins,et al.[1], and Moiseev et al [2]. As was shown in Figures 5 and 6 of this investigation, tangential intensities were found to be nearly 30 to 40% higher than the axial intensities. Contraction of the flow resulted in a 10% decrease in both components of turbulence intensity. With the decreased intensity, it was found that the axial length scale increased 25%.

Hanson [8], who is one of the earliest to investigate inlet turbulence, measured the axial and tangential intensities to be 0.9% and 2.5% of the mean flow, respectively. The axial length scale of this turbulence was found to be 500 cm. Such a high tangential intensity and long length scale can be attributed to the ingestion and stretching of large scale atmospheric turbulence. The upper limit on the characteristic size of a turbulent eddy in this case is on the order of the thickness of the planetary boundary layer. Therefore, only a qualitative comparison can be made showing that the tangential intensity is higher than the axial intensity. No quantitative results can be drawn.

Robbins and Lakshminarayana's [1] data is similar to the present investigation, even though the intensities are slightly higher. The higher turbulence intensities measured are believed to be the result of operating at a higher flow coefficient and because a different anechoic enclosure was used.

Data on turbulence levels by Moiseev et al (Table III) indicate that the axial intensities are 2.5% of the mean flow and the tangential intensities are 0.5% near the center of the annulus. The higher axial intensity relative to the tangential intensity was the result of a fully developed boundary layer being present on the inner wall of the annulus. The presence of this boundary layer is also seen to reduce the axial length scale of ingested turbulent eddies. Finally, Moiseev, et al. in addition to the long eddies, measured a much shorter eddy length scale and attributed this length scale to the eddies associated with the boundary layer. Since this investigation did not measure any small eddies in the inflow, it can be concluded that the short eddies measured by Moiseev et al. were developed in the wall boundary layer.

Acoustic Data and Correlation

The far field spectrum of the noise of the rotor with the configuration shown in Figure 3 (17 blades, short centerbody, ϕ = 0.75, 5440 rpm), with the microphone at 76.2 mm from the inlet, is shown in Figure 10 for both the grid and no grid case. This provides a dramatic illustration of the effect of elongated or long eddies. With no grid, the maximum length scale and the axial turbulence intensity at station 1 are 242 cm and 0.06, respectively. The corresponding values for the grid case are 22 cm and 0.10, respectively. It is evident that a 10 dB decrease in noise level brought about by placing the grid is mainly due to the shortened length scale, even though the turbulence intensity is increased. The noise intensity is decreased by 10 dB, while the length scale decreased by a factor of 10. Thus, it is evident that the process described is this paper, namely the elongation of the eddies through the contraction, is a major contributor to the noise level. This points out the need for a modification of existing theories to include non-isotropy and long length scales in the turbulent description.

DISTURBANCE DUE TO STRUT WAKE AND VORTEX FLOW

Aerodynamic Data and Interpretation

Results of the strut wake measurements are shown in Figures 11 and 12. The velocity component U_{xr} is nondimensionalized by the free stream axial velocity and plotted as a function of the normalized tangential distance Y. It should be remarked here that $U_{xr} \simeq U_x$, since the radial velocities are small. The single sensor hotwire used in these experiments senses U_{xr}, the resultant of axial and radial velocities. The symmetry of the wake in these figures was expected since the strut profile is symmetric and was operated at zero incidence to the mean flow.

In Figure 11a, the decay of the strut wake at a radius of $r/r_t = 0.75$ for the case of no grid is shown. The velocity defect (Λ) was observed to decrease from $\Lambda = 0.32$ at $Z = 0.18$ to a value $\Lambda = 0.06$ at $Z = 1.8$. With the decay of the velocity defect, the wake spread from a width of $L_w = 0.24$ to a width $L_w = 0.57$. As illustrated in Figure 11b, the installation of the grid did not significantly alter the velocity profile of the wake. The variation of velocity defect and wake width with strut spacing were the same as with no grid present. For both the grid and no grid case, the length of the centerbody had no effect on the wake profile at this radius.

Measurements from this investigation of the decay of the velocity defect were plotted against data from the study by Lakshminarayana and Davino [9] in Figure 12. The comparison indicates that the trend shown by the data of Lakshminarayana and Davino was closely matched by this investigation. The higher velocity defect close to the trailing edge was the result of the low guidevane solidity.

The wake profiles at a radius of $r/r_t = 0.54$ (which is very near the centerbody) are shown in Figures 13a and 13b. Again, the profiles are symmetric except for the rotor/strut spacings $Z = 0.9$ on the 26.35 cm centerbody and $Z = 1.8$ on the 47.63 cm centerbody. For both these cases, the boundary layer on the centerbody is on the order of 0.3 cm thick. The effect of vortex flow is clearly seen in these figures. As reported by Barber [3], the thin boundary layer allows low momentum flow to collect at the trailing edge of the root section of the strut. Since this flow cannot support the adverse pressure gradient developing on the strut, flow separation is likely to occur on the strut.

The velocity defect of the profiles in Figure 13a were found to be 20% higher than those at the strut midspan. This increase can be attributed to the contribution made to the velocity vector by the radial component of velocity. The radial or spanwise velocity generated by vortex flow is responsible for the higher velocity (than the free stream region) near the edge of the wake. Again, use of the grid altered the wake decay characteristics only slightly as shown in Figure 13b.

The vortex flow generated near the centerbody region, Figure 13a and 13b, will have a substantial influence on the noise generation. This provides not only periodic distortion but also the random distortions to the subsequent rotor for the case of the grid being installed with the exception of the axial spacing Z = 0.18.

Based on the velocity gradient in Figure 13, a calculation was made of the approximate strength of the vortex flow. These calculations are compared in Figure 12 to the vortex flow strength predicted using the theory due to Hawthorne [10, 11]. The strength of the vortex flow was normalized with respect to the strongest vortex flow case (47.63 cm centerbody, Z = 0.18). The boundary layer was normalized with respect to the thickest boundary layer. As illustrated in Figure 12, the trend exhibited by the calculated vortex flow strength for each configuration agrees well with theory. The prediction is based on the integration of Hawthorne's [11] expression for vorticity along the stream tube near the surface where the strength is likely to be maximum. The normal vorticity used in the calculation is based on measured inlet velocity profile.

The measured turbulence profiles of the strut wake are shown in Figure 15 for the radius ratio r/r_t = 0.75. In Figure15a, the wake centerline turbulence intensity at Λ = 1.8 is nearly equal to the peak intensity at Z = 0.18. This decay rate, compared to the rate of decay of the velocity defect, indicates that for this configuration, the wake turbulence decays 20% slower than the velocity defect. The length of the centerbody did not alter the intensity at the axial distance of 0.18. The effect of grid generated turbulence on the turbulence intensity profiles is shown in Figure 15b. Installation of the grid increases free stream turbulence intensities from 2% to 5%. The turbulence intensity levels at the wake centerline also increase when a grid is placed.

Illustrated in Figure 16 are the guidevane wake turbulence profiles at a radius of r/r_t = 0.54 with no grid installed. The appearance of the peaks on either side of the guidevane wake peak are the result of vortices. The turbulence intensity of these vortices was measured to be 12% of the flow velocity for an axial spacing of Z = 0.18 for both the long and short centerbodies. This level of turbulence was on the order of the wake centerline turbulence intensity of 13%. Movement downstream to Z = 0.9 results in a 25% decay of the wake centerline turbulence for the long and short centerbody.

Installation of the grid again results in an increase in the intensity of turbulence as seen in Figure 16b. The wake centerline turbulence levels, when compared to the no grid case, decay twice as fast. This decay rate also applies to the intensities in the vortex flow region.

Comparing Figure 16a with Figure 13a, where the velocity data is plotted, it is clear that the core of the vortex region is located near y = $\pm$1.5, where the velocity is minimum and the turbulence intensity is maximum. The edge of the vortex is located approximately at y = $\pm$0.5, where the velocity is maximum and the turbulence intensity is minimum.

The wake and vortex flow regions coexist in the wall region, thus resulting in a complex distortion (both random and periodic) of the inflow into the rotor. This should contribute not only to the pure tone noise, but also to the broadband noise of the rotor. The turbulence intensities at Z = 0.18, r/r_t = 0.54 (Figure 16a) are of the same order of magnitude as the velocity defects (Figure 13a).

Acoustic Data and Interpretation

The spectrum of background noise was measured with the rotor removed and the auxiliary fan running at its test speed. The background noise level was found to be at least 10 dB below the rotor noise spectrum and, therefore, the signal-to-noise ratio was considered acceptable. The directivity pattern for the 17-bladed rotor was also measured with the microphone located at the radial position 76.2 cm upstream of the inlet (Figure 3). The results are shown in Figure 17. Since no lobed pattern was measured, the sound levels measured along the annulus centerline were considered representative for all angles.

Sound spectra measured for the 47.63 cm centerbody with and without grid are shown in Figure 18a and 18b. With no struts present, the first, second, and third harmonics of blade passing frequency (BPF = 1541 Hz) were measured at levels of 92 dB, 78 dB, and 74 dB respectively. Installation of the four struts at the greatest axial spacing of Z = 1.8 resulted in a slight (2 dB) increase in the first harmonic with no increase being measured for the second and third harmonics. The addition of the struts also produced peaks at the first three harmonics of the strut passing frequency, of 363 Hz. The SPL of these peaks was 74 dB. Movement of the struts to the position Z = 0.9 resulted in a 4 dB increase in the second BPF and no noticeable change in the first and third harmonics of BPF. A 4 dB increase in the first harmonic of the strut passing frequency was also measured. At the Z = 0.18 spacing, the first and second harmonics of BPF did not change, but the third harmonic increased by 5 dB. These results seem to indicate that the strut wake has very little effect on the noise generation in this particular case, i.e. the dominant source in still the inlet turbulence. Also, the second harmonic of strut passing frequency showed a 3 dB increase, while the first and third harmonics were constant. The broad peak centered at a frequency of 1.8 kHz was the result of a blade vibration. The broadband level was constant at 65 dB and was not altered by strut spacing.

The effects of the grid on the rotor noise spectra, Figure 2, are shown in Figure 18b. Two results are immediately apparent; the first was the decrease in number and magnitude of BPF and strut passing frequency harmonics, and the second was the broadening of the peak at the first BPF of 1541 Hz. Beginning with the no strut case; the levels of the first through third harmonics of BPF were 81 dB, 73 dB, and 73 dB, respectively. Thus, the grid reduced the first BPF harmonic by approximately 10 dB and the second harmonic by 5 dB. Addition of the struts at an axial distance of Z = 1.81 resulted in only a 2 dB increase in the first BPF and no increase in the second and third harmonics. No peaks were measured above the broadband level for the strut passing frequency. This was

seen again for the case dominated by inlet turbulence. Movement of the struts to Z = 0.9 resulted in a dramatic increase in the first harmonic of BPF to 94 dB. Increases of 5 dB and 2 dB were also measured for the second and third harmonics of BPF. At this spacing, the first and second harmonics of the strut passing frequency appear above the broadband noise at a level of 75 dB. The closest spacing of Z = 0.18 results in a decrease in the level of the first harmonic of BPF to 83 dB. The levels of the second and third harmonics increase to levels of 85 dB and 78 dB, respectively. No change was noticed in the first and second harmonics of strut passing frequency. Finally, around the first harmonic of BPF a 5 dB increase in the broadband signal was measured as a result of the grid induced turbulence. This turbulence also increased the entire broadband level by 3 dB to 68 dB.

The effects of the shorter (26.35 cm) centerbody with no grid are shown in Figure 19a. The difference between the longer and the shorter centerbodies, in so far as the flow is concerned, is mainly the alteration of the strength of the vortex flow. The inlet turbulence properties and the wake flow field should be identical in both cases. With no struts installed, a SPL of 90 dB for the first harmonic and 72 dB for the second and third harmonics of BPF were recorded. With the struts at Z = 0.9, the first harmonic increased to 93 dB and the second harmonic of BPF increased to 81 dB. No change occurred at the third harmonic. The levels of the first, second, and third harmonics of strut passing frequency were 77 dB, 75 dB and 73 dB, respectively. Movement of the strut to Z = 0.18 caused no change in the BPF harmonics. The first and second harmonics of strut passing frequency, however, did increase by 2 dB each.

The measured spectra with the grid installed are shown in Figure 19b. Without struts, the level of the first BPF was 82 dB. At Z = 0.9, the first, second and third harmonics were 86 dB, 78 dB and 74 dB, respectively. Moving the struts closer resulted in an increase of 4 dB in the first BPF harmonic. Increases of 3 dB and 9 dB were measured for the second and third BPF harmonics. The first and second strut passing frequency harmonics appeared at this spacing with sound pressure levels at 75 dB. The broadband level was measured at 68 dB.

Correlation of Acoustic Data

In the configuration used by the authors, there are three sources of flow disturbances that can generate coherent noise, as follows: (1) long eddies in the inlet turbulence, (2) turbulence and velocity defects in the strut wake, and (3) turbulence and velocity distortion in the vortex flow at the root of the strut. The purpose of this section is to evaluate the relative importance of these effects, based on physical phenomena, flow-noise correlation and existing theories. In this section, the variation of the dB level of the first harmonic of BPF is correlated with the measured changes in such parameters as wake velocity profile, wake velocity defect, wake turbulence, vortex flow strength, and the inlet turbulence. The measured sound pressure levels of the first harmonic of BPF were also compared to the predicted levels obtained by an analytical method due to Homicz [12] and an unsteady thrust analysis due to Thompson [13] to determine which of these sources are dominant sources of rotor noise.

The relative dB levels of the first, second, and third harmonics of BPF are shown in Figure 20a and 20b for the grid and no grid case, respectively. A comparison of the theories with the measured SPL of the first BPF is shown in Figure 21. Homicz's theory, which models the strut wake based on an isolated airfoil wake decay model, predicts that a 20 dB drop should occur with the change in axial separation between the strut and the rotor used in this experiment. This drop in SPL was not measured in either the grid or the no grid case. Homicz's program was then modified to exclude noise due to potential flow effects and noise due to rotor blade passing the strut, in an attempt to determine only the noise due to the rotor operating in the strut wakes. Results indicate that, although a lower SPL was obtained, the predicted dB change with separation was much higher than measured.

A second attempt to correlate the strut wake with the sound pressure level was conducted by calculating the unsteady thrust of the rotor by using an analysis due to Thompson [13]. Input of this technique required 360° wake surveys at three radii (r/r_t = 0.54, 0.75 and 0.95). This data is similar to those presented in Figures 11 - 16, with the exception of the additional data due to the other three strut wakes. Each wake survey was Fourier analyzed to determine the harmonic coefficients. These derived Fourier coefficients were then used to obtain the unsteady rotor thrust. As shown in Figure 21, the relative dB drop in the unsteady thrust with axial spacing indicates a 10 drop. This confirms the earlier conclusion that the velocity defect due to the strut wake was not the major noise source.

An attempt was made to estimate the trend in the tonal noise generated due to various sources using the experimental flow data. Four sources under consideration were; inlet turbulence, wake velocity defect, maximum turbulence intensity in strut wakes and the strength of the vortex flow. The noise due to the mean velocity defect should vary as 20 log Λ, when all other blade and flow parameters are held constant. Similarly, the noise due to wake turbulence and the vortex flow should vary as 20 log $\left[\sqrt{\overline{u^2}}/U\right]$ and 20 log ξ, respectively. The trends estimated from such a calculation are shown in Figure 22 and are compared with the measured data. While the measured tonal intensity variation is only 2 dB for the range of Z = 0.18 to 1.8, the variation estimated due to various sources are substantial. This seems to indicate that the noise due to long eddies in the inlet turbulence still dominate. The observed variation in the tonal noise intensity at BPF with strut spacing is within the experimental accuracy. Further, the length scale measurements inside the wake indicate that the long length scales present at the inlet are unaffected as they pass through the struts (both free stream and boundary layer).

Installation of the grid has been shown to eliminate the long length scales and is, therefore, more likely to reveal changes in the SPL due to changes in wake parameters. It is evident in Figure 22b that, of the three parameters plotted against the SPL, only the vortex strength shows a similar trend. The vortex strength at an axial spacing of Z = 1.8 could not be calculated, it is expected that it would have been less than at Z = 0.18. Therefore, the wake velocity defect and turbulence intensity are not strong contributors to the rotor noise spectrum.

To determine the effect of vortex flow on the rotor noise spectra, comparisons are made between the two centerbodies at identical axial spacings for the case with grid, where the eddies are short. Long eddies are major sources of noise in such a static facility. It may overshadow all other sources. In Figure 23, the dB change in the vortex flow strengths were calculated for the two spacings Z = 0.9 and Z = 0.18 for the long and short centerbodies and plotted against the SPL changes. The wake parameters of velocity profile, velocity wake defect and wake turbulence are constant between the two centerbodies for a given strut spacing, therefore, good agreement is seen between the vortex flow strength changes and the SPL. This indicates that this type of vortex flow noise could be appreciable in some rotors.

CONCLUSIONS

The following major conclusions can be drawn from the research reported in this paper:

(1) The hypothesis by earlier investigators on the effect of a static facility on the elongation of eddies has been confirmed. The measurements indicate that eddies are stretched as much as ten times their original length. This should depend on the contraction ratio and the inflow turbulence properties.

(2) In the presence of these long eddies, the strut wake (mean velocity defect) is not a major source of noise.

(3) The unsteady thrust computed from the measured mean velocity wake profiles does not correlate well with the trend exhibited by the pure tone noise. This is the basis of the conclusion that, in this particular case, the inflow turbulence and vortex flow dominate the noise generation.

(4) The vortex flow generated near the intersection of the centerbody and strut seems to be a dominant source of noise when the inlet turbulence effects are small (e.g. short eddies). The tonal noise correlates well with the strength of the vorticity for the case with a grid.

(5) These conclusions are valid for low speed turbomachinery. At higher speeds, the relative importance of these sources may change.

REFERENCES

1. Robbins, B. and Lakshminarayana, B., "Effect of Inlet Turbulence on Compressor Noise," Journal of Aircraft, Vol. 11, No. 5, pp. 273-281, 1974.

2. Moiseev, N., Lakshminarayana, B., and Thompson, D. E., "Noise Due to Interaction of Boundary Layer Turbulence with a Compressor or a Propulsor Rotor," Journal of Aircraft, Vol. 15, No. 1, January 1978, pp. 53-61.

3. Barber, T. J., "An Investigation of Strut-Wall Intersection Losses," AIAA 16th Aerospace Sciences Meeting, AIAA Paper No. 78-205, January 16.18, 1978.

4. Ribner, H. S., and Tucker, M., "Spectrum of Turbulence in a Contracting Stream," NACA Report 1113, 1952.

5. Bekofske, K. L., Sheer, R. E., and Wang, J. C. F., "Fan Inlet Disturbances and Their Effect on Static Acoustic Data," Journal of Engineering for Power, Vol. 99, 1977, pp. 608-616.

6. Shaw, Loretta M., Woodward, Richard P., Glasner, Frederick W., and Dastoli, Benjamin J., "Inlet Turbulence and Fan Noise Measured in an Anechoic Wind Tunnel and Statically with an Inlet Flow Control Device," NASA TM-73723, October 1977, (AIAA Paper 77-1345).

7. Shaw, Loretta M., Private Communication.

8. Hanson, D. B., "Spectrum of Rotor Noise Caused by Atmospheric Turbulence," Journal of Acoustical Society of America, Vol. 56, No. 1, pp. 110-126, July 1964.

9. Lakshminarayana, B., and Davino, R., "Mean Velocity and Decay Characteristics of the Guidevane and Stator Blade Wake of an Axial Flow Compressor," Journal of Engineering for Power, Volume 102, No. 1, pp. 50-60, 1980.

10. Hawthorne, W. R., "Secondary Circulation in Fluid Flow," Proceedings of the Royal Society, London, England, Series A., Vol. 206, pp. 374-387, 1951.

11. Hawthorne, W. R., "Secondary Flow About Struts and Airfoils," Journal Aero Sci., Vol. 21, pp. 508-608, 1954.

12. Homics, G. F., Ludwig, G. R., and Lordi, J. A., "Theoretical and Experimental Studies of Discrete-Tone Rotor-Stator Interaction Noise," Progress in Aeronautics and Astronautics, Vol. 44, pp. 3-22, 1975.

13. Thompson, D. E., "Propeller Time-Dependent Force Due to Nonuniform Flow," a Doctor of Philosophy thesis in Aerospace Engineering, The Pennsylvania State University, 1976.

Table 1

EXPERIMENTAL CONFIGURATIONS AND BPF TONE LEVELS

Length of Centerbody	Probe to Strut Distance Z[1]	Grid	1st BPF Tone Level SPL	2nd BPF Tone Level SPL	3rd BPF Tone Level SPL
47.63 cm	NS[2]	No	92	78	74
"	NS	Yes	81	73	73
"	0.18	No	95	83	80
"	0.18	Yes	87	84	78
"	0.91	No	95	83	75
"	0.91	Yes	94	78	74
"	1.82	No	94	79	74
"	1.82	Yes	83	72	72
26.35 cm	NS	No	90	72	71
"	NS	Yes	82	NP[3]	NP
"	0.18	No	93	80.5	78
"	0.18	Yes	90	81	83
"	0.91	No	93	80.5	73
"	0.91	Yes	86	77.5	74

[1]Z is the distance from strut trailing edge to rotor leading edge nondimensionalized by the chord for acoustic measurements.

[2]No struts present (noise due to wall boundary layer and inflow turbulence only).

[3]Not present (NP).

25 February 1980
RT:BL:DET:cac

Table 2

LENGTH SCALE MEASUREMENTS

Station 1 6.7 cm Upstream of Rotor			Station 2 31.4 cm Upstream of Rotor			Station 3 10.3 cm Upstream of Inlet		Station 4 17.6 cm Upstream of Inlet	
Radial Location r/r_t	Axial Length Scale		Radial Location r/r_t	Axial Length Scale		ARC Location (deg)	Axial Length Scale (cm)	ARC Location (deg)	Axial Length Scale (cm)
	No Grid (cm)	Grid (cm)		No Grid (cm)	Grid (cm)				
.51	188	7.26	0.00	137	9.23	90°*	57	90°*	16
.54	210	7.42	0.20	133	7.87	70°	53	80°	22
.57	210	7.73	0.29	127	8.28	50°	113	70°	18
.60	179	8.05	0.35	128	8.36	30°	77	60°	27
.63	136	8.11	0.41	131	8.03	8°	93	50°	25
.66	136	8.32	0.47	129	7.32			40°	27
.68	148	7.54	0.52	129	7.91			30°	34
.71	160	7.22	0.58	143	7.56			20°	43
.74	190	7.61	0.64	131	7.75			10°	31
.77	181	8.87	0.70	203	8.46			0°	30
.80	163	7.81	0.76	180	8.86				
.83	165	8.31	0.81	130	8.34				
.86	210	10.40	0.87	155	8.02				
.89	208	12.80	0.93	193	11.50				
.92	242	17.60	0.96	139	12.40				
.95	179	22.00							
.97	209	17.40							

*Inlet Annulus Centerline

25 February 1980
RT:BL:DET:cac

Table 3

SUMMARY OF RESULTS OF PREVIOUS INVESTIGATIONS

	Facility	Turbulence	Annulus Diameter (d)	Annulus Height Above Floor	Probe Type and Location	$\frac{L_x}{L_\theta}$	U_x m/sec	$\frac{\sqrt{u^2}}{U_x}$	$\frac{\sqrt{v^2}}{U_x}$	$\frac{M_t}{M_a}$	ϕ	N	$\frac{h}{r_t}$
(1) Shaw, Woodward, Glasner, and Wang (Reference 6)	Fan	Room	50.8 cm	2d[1]	"X" Array Hotfilm 0.5d Downstream of Inlet No Centerbody	$\frac{9.8\text{-}13.8d}{\text{N. A.}^2}$	116.0	0.5	5.0-5.8%	0.6	.73	15	0.46
(2) Bekofske, Sheer and Wang (Reference 5)	Fan	Room	50.4 cm	5d	"X" Array Hotfilm 1.0d Downstream of Inlet No Centerbody	Porous Wall $\frac{4.4\text{-}8.9d}{.6\text{-}.3d}$ Non Porous $\frac{17.8\text{-}30d}{1.49\text{-}0.9d}$	476.0	1.7 1.7	.6-1.4% 1.2-1.7%	$\frac{1.24}{.85}$	1.09	44	0.50
(3) Robbins and Lakshminarayana (Reference 1)	Fan	Room	17.78 cm	8.5d	"X" Array Hotwire Annulus 4.07d Downstream of Inlet	$\frac{\text{N. M.}}{\text{N. M.}}$	56.81	1.9%	2.5	$\frac{.15}{.17}$	1.14	17	0.5
(4) Moiseev, Lakshminarayana and Thompson (Reference 2)	Fan	Room	17.78 cm	8.5d	"X" Array Hotwire Annulus 3.45d Downstream of Inlet	$\frac{4.82\text{-}6.58d}{.45d}$	39.0	2.5%	0.5%	$\frac{.15}{.11}$	.75	17, 10	0.5
(5) Hanson (Reference 8)	Inlet Shroud and Center-Body	Atmosphere	53.3 cm	8.0d	"X" Array Hotwire Annulus 0.5d Downstream of Inlet	$\frac{50\text{-}100d}{.14d}$	73.15	0.9%	2.5%	$\frac{.21}{\text{N.A.}}$	N.A.	NA	0.5

25 February 1980
RT:BL:DET:cac

Table 3 (Continued)

	Facility	Turbulence	Annulus Diameter	Annulus Height Above Floor	Probe Type and Location	$\frac{L_x}{L_\theta}$	U_x m/sec	$\frac{\sqrt{u^2}}{U_x}$	$\frac{\sqrt{v^2}}{V_x}$	$\frac{M_t}{M_a}$	ϕ	N	$\frac{r}{r_t}$
(6) Same as Above	Fan	Room	17.78 cm	8.5d	1.0d Upstream of Inlet	.9-1.69d	1.8	1.0%	0.8-1.0%	.15/.11	.75	17	0.5
(7) Trunzo, Lakshminarayana and Thompson (This Investigation)	Fan	Room	17.75 cm	8.5d	"X" Array Hotwire 0.58d Upstream of Inlet	3.12-6.58d / N. M.	4.04	1.5%	2.0-2.5%	.15/.11	.75	17	0.5
(8) Trunzo, Lakshminarayana and Thompson (This Investigation)	Fan	Room	17.78 cm	8.5d	"X" Array Hotfilm 2.68d Downstream of Inlet No Centerbody	7.31-11.4d / N. M.[3]	28.4	1.1-1.7%	1.3-1.7%	.15/.11	.75	17	0.5
(9) Trunzo, Lakshminarayana and Thompson (This Investigation)	Fan	Room	17.78 cm	8.5d	"X" Array Hotwire Annulus 4.07d Downstream of Inlet	7.5-13.6d / N. M.	36.9	1.0-1.5%	1.3-1.6%	.15/.11	0.75	.17	0.5

[1]Symbol "d' refers to the outer diameter of the annulus. All distances are expressed in terms of annulus outer diameter.

[2]Not Available (N. A.).

[3]Not Measured (N. M.).

25 February 1980
RT:BL.:DET:cac

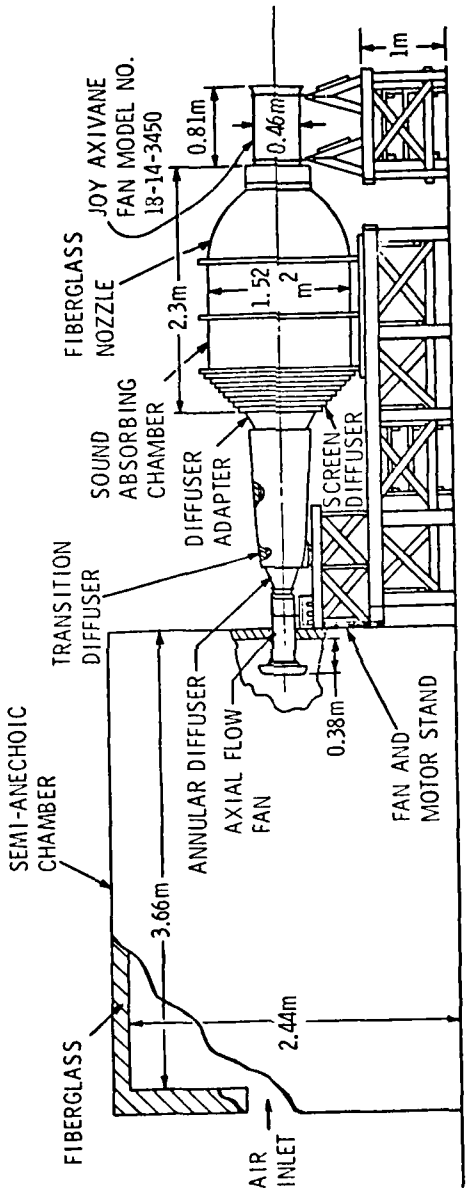

Figure 1. Aeroacoustic Test Facility and Anechoic Chamber

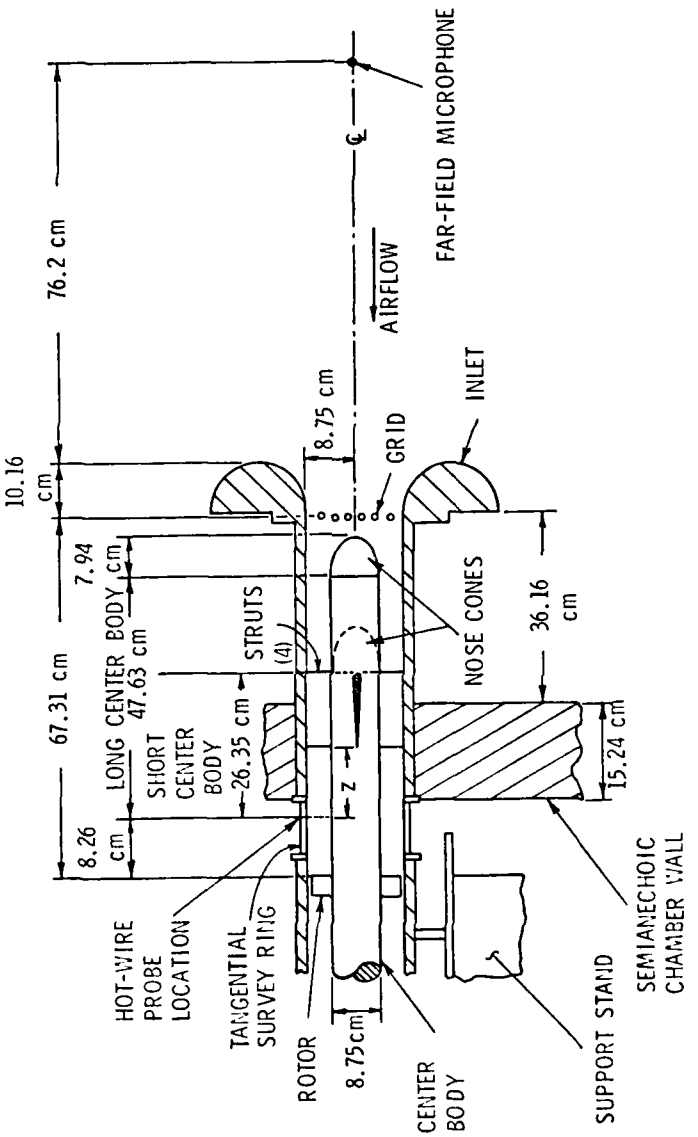

Figure 2. Planview of Inlet Showing Strut Position

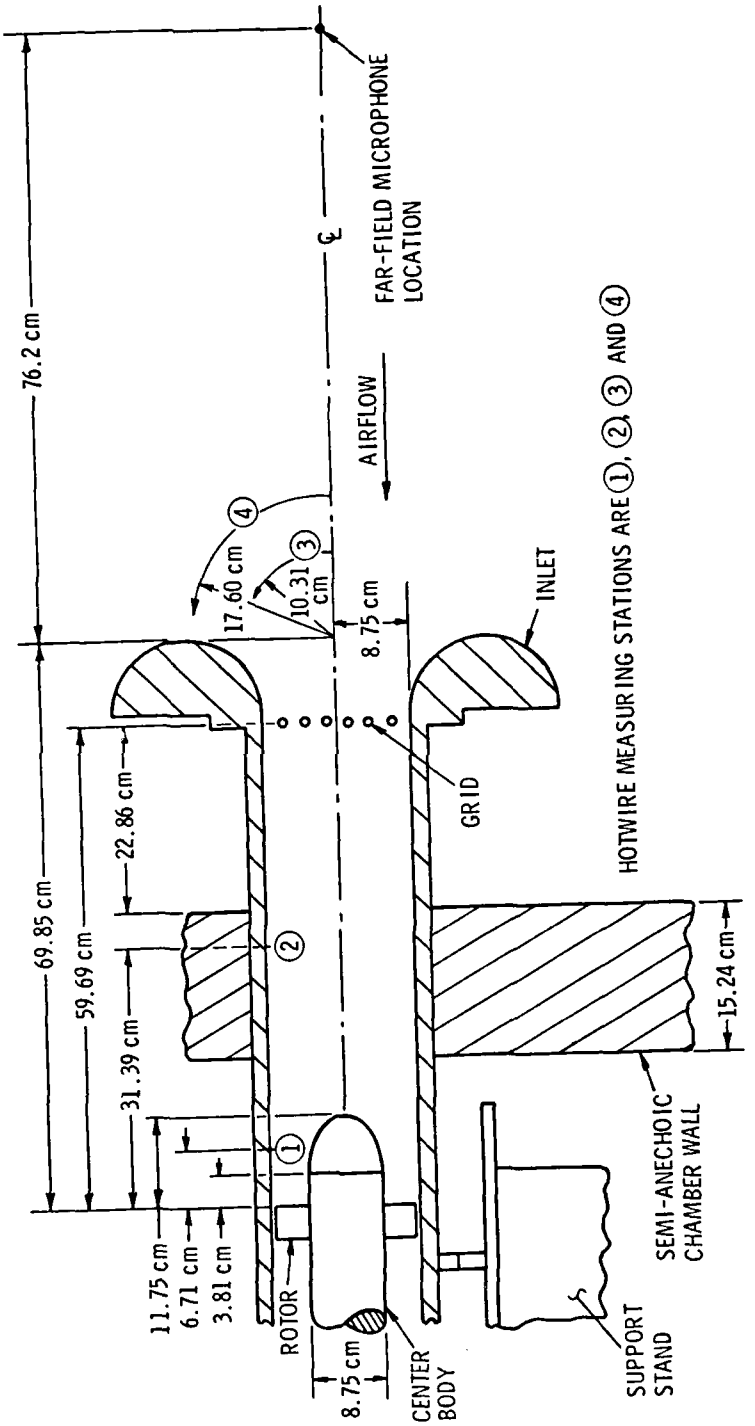

Figure 3. Planview of Inlet Showing Measuring Stations

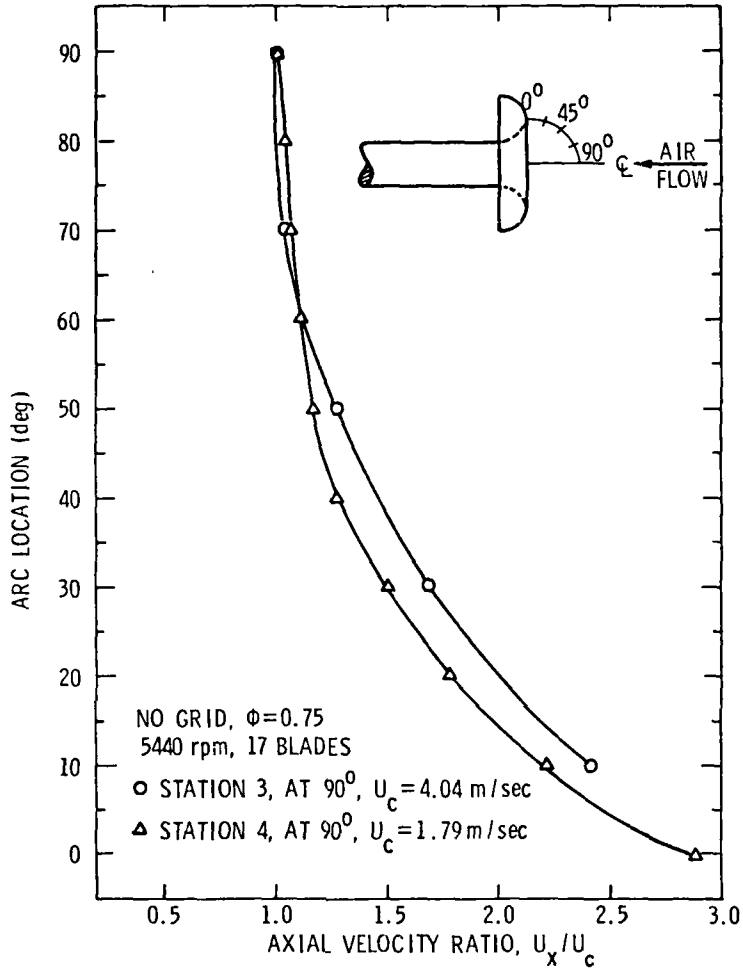

Figure 4a. Axial Velocity Profiles

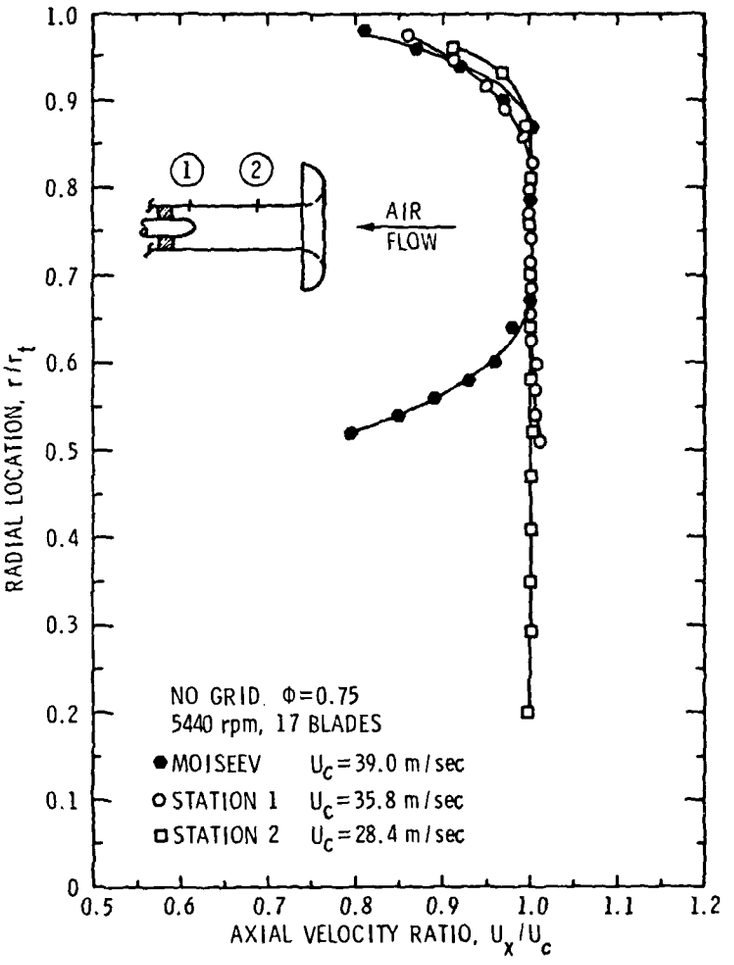

Figure 4b. Axial Velocity Profiles

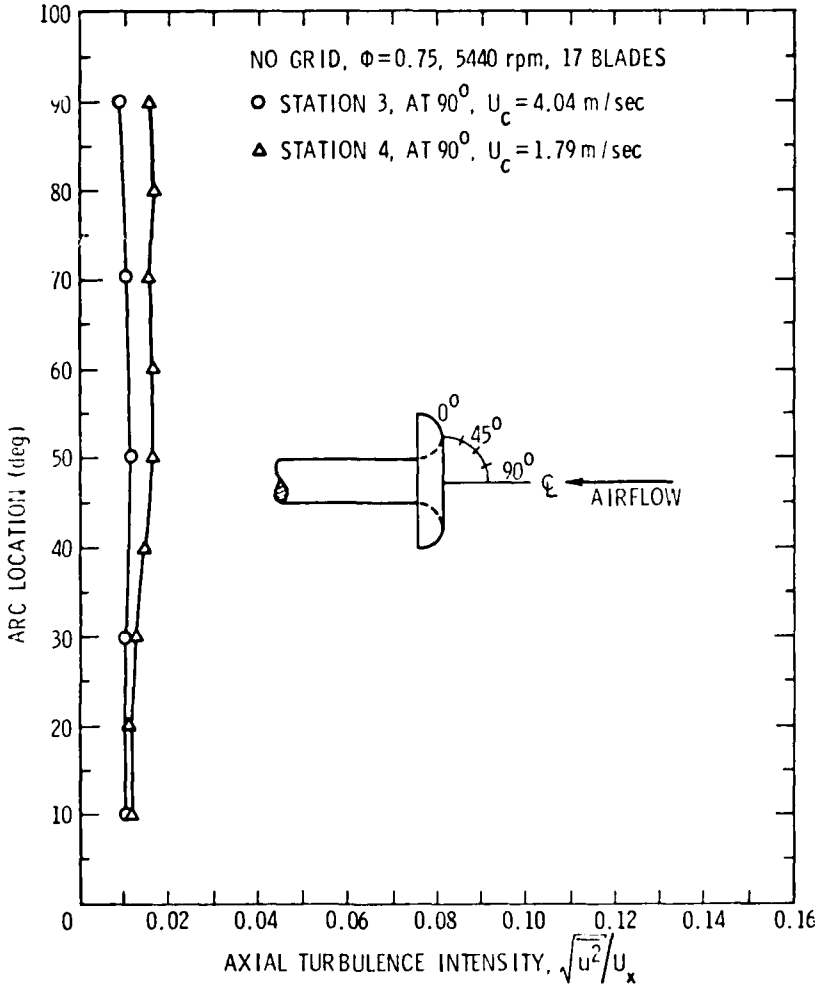

Figure 5a. Turbulence Intensity Profiles Upstream of the Inlet

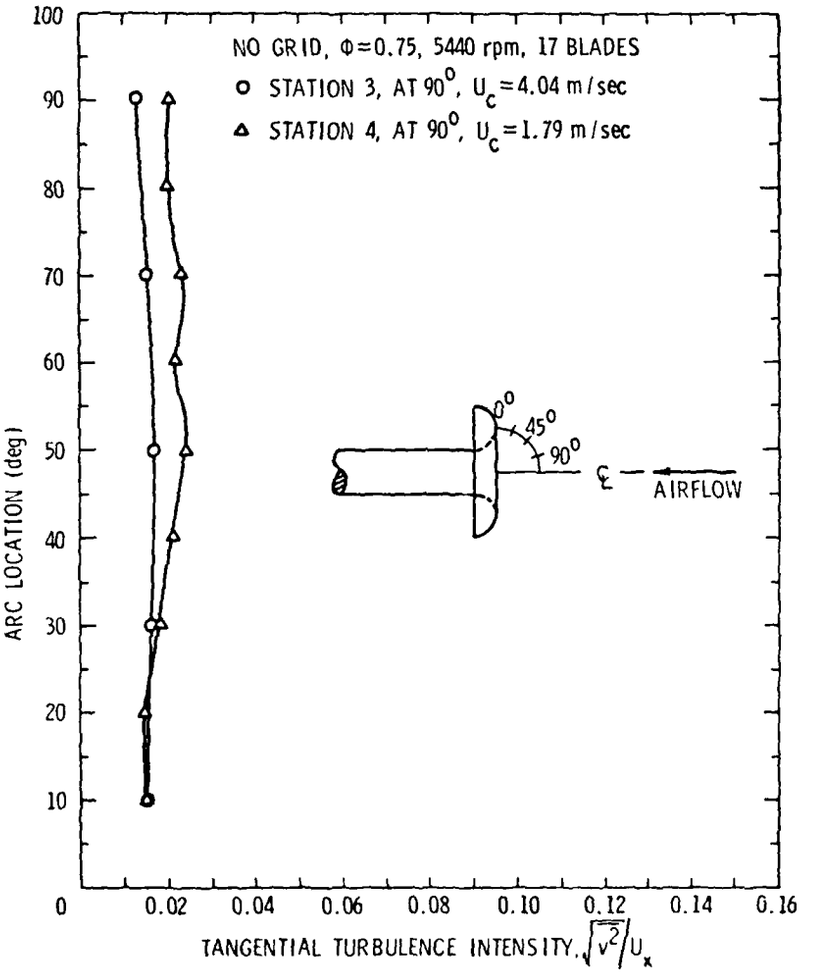

Figure 5b. Turbulence Intensity Profiles Upstream of the Inlet

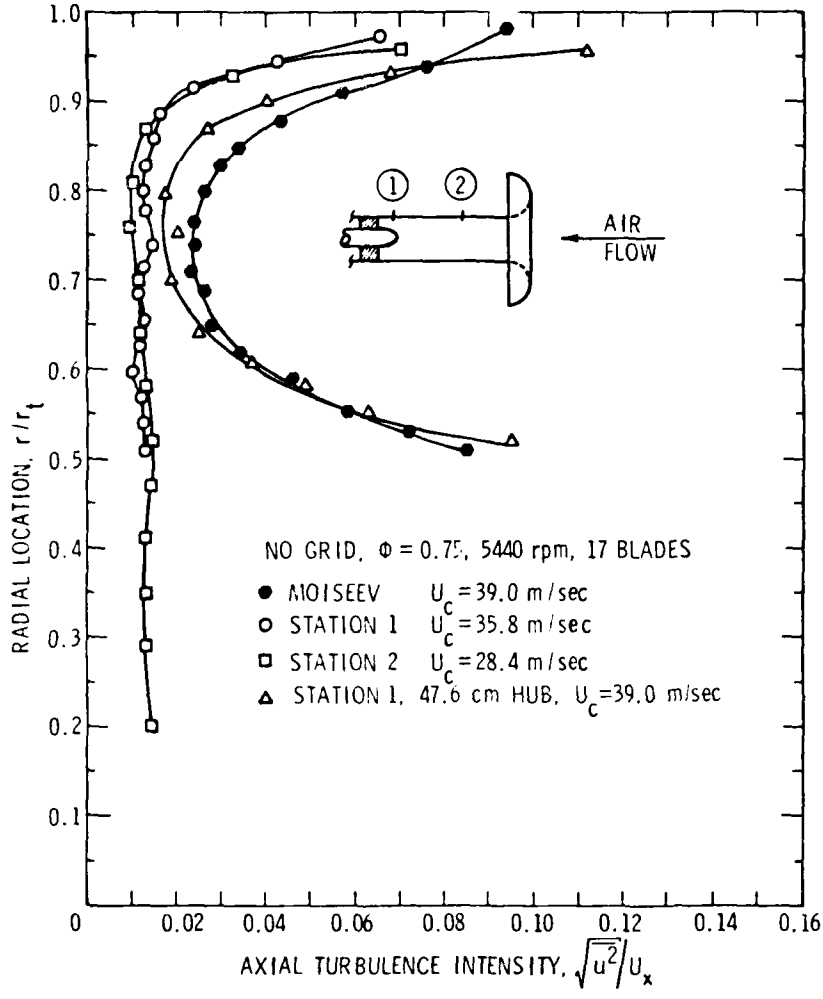

Figure 6a. Turbulence Intensity Profiles Downstream of the Inlet, No Grid Installed

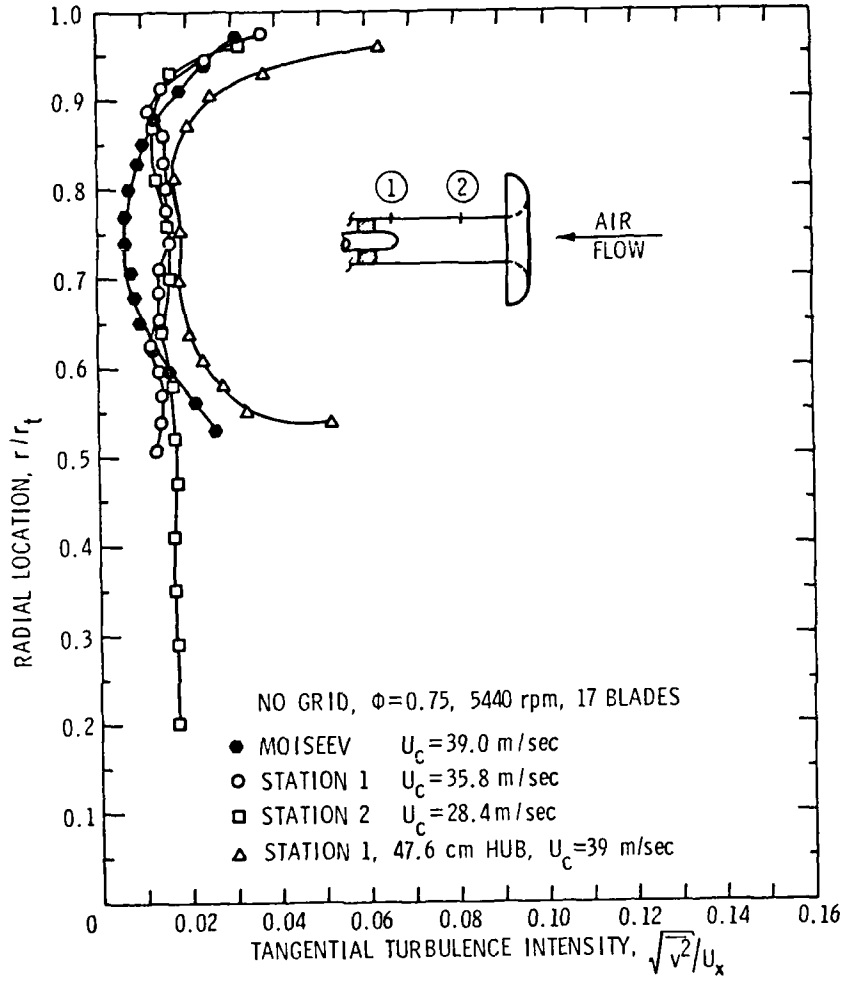

Figure 6b. Turbulence Intensity Profiles Downstream of the Inlet, No Grid Installed

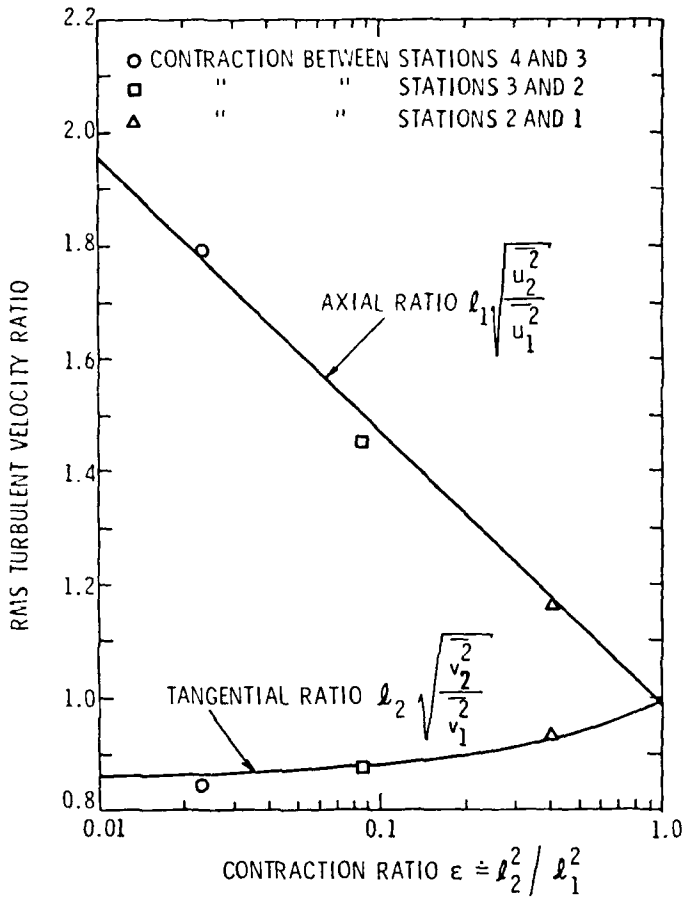

Figure 7. Comparison of Data to Theory by Ribner and Tucker

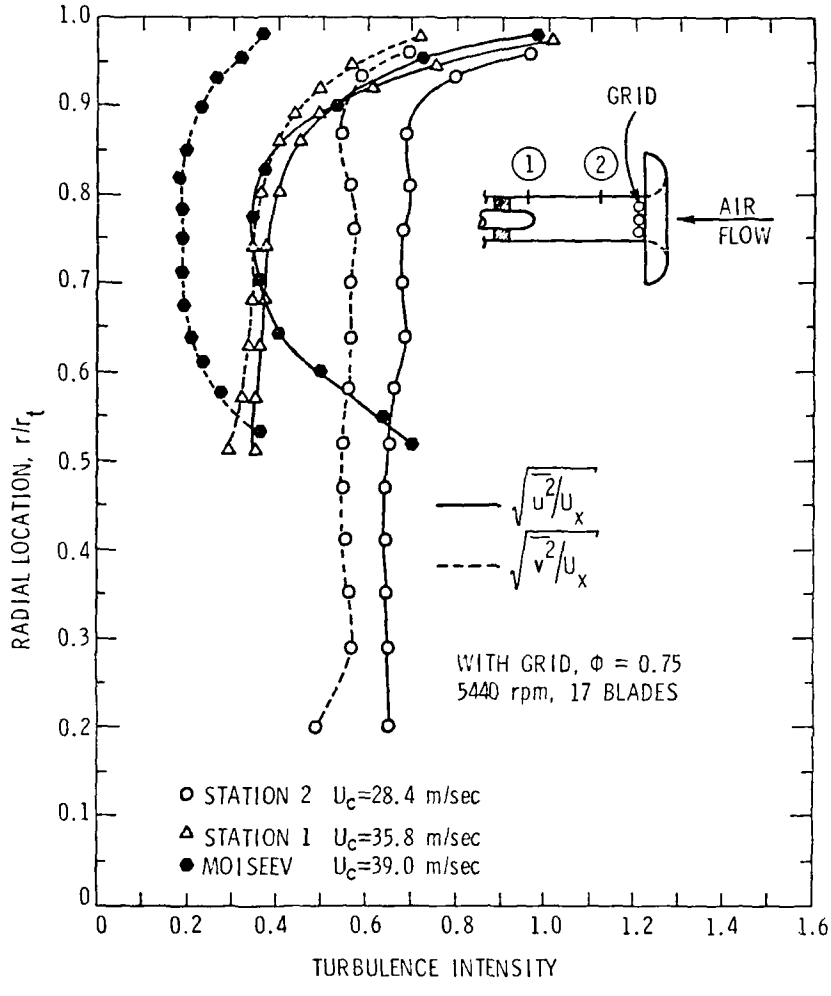

Figure 8. Turbulence Intensity Profiles Downstream of the Inlet with Grid Installed

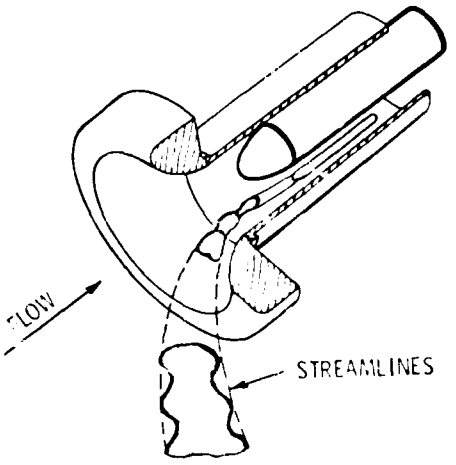

Figure 9. Schematic of Turbulent Eddies

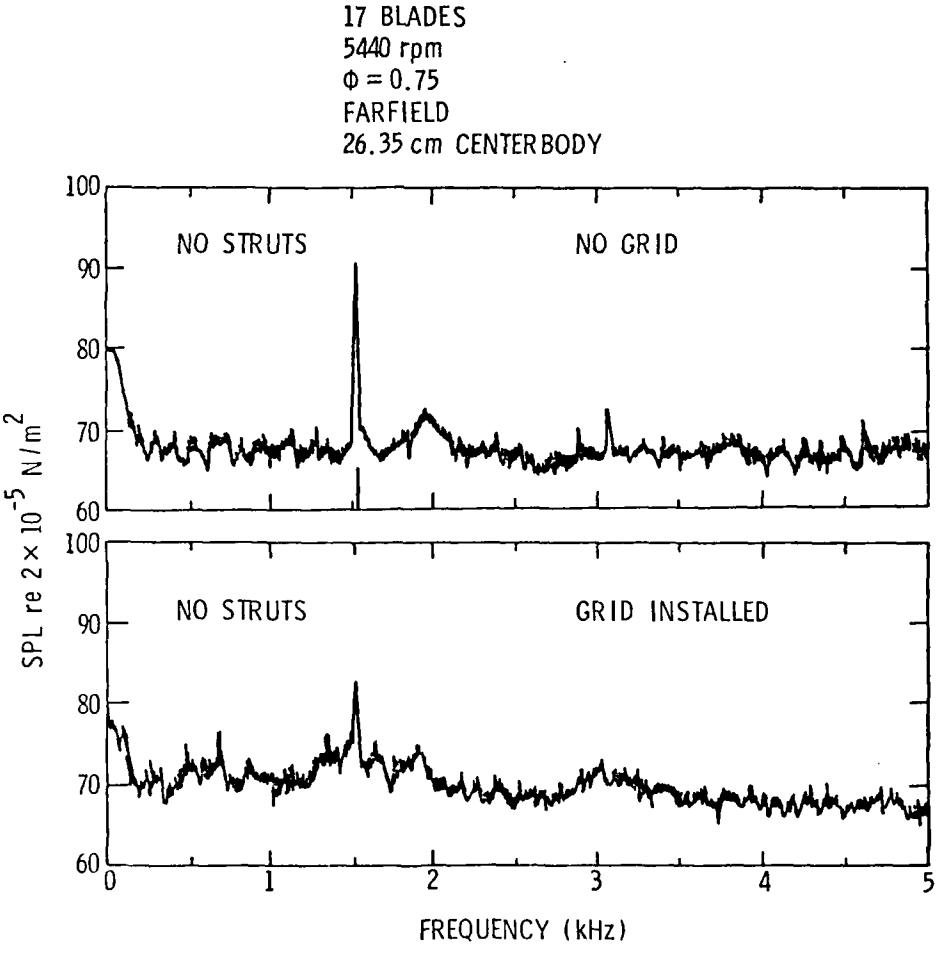

Figure 10. Spectra with Short Centerbody and Long Inflow Eddies

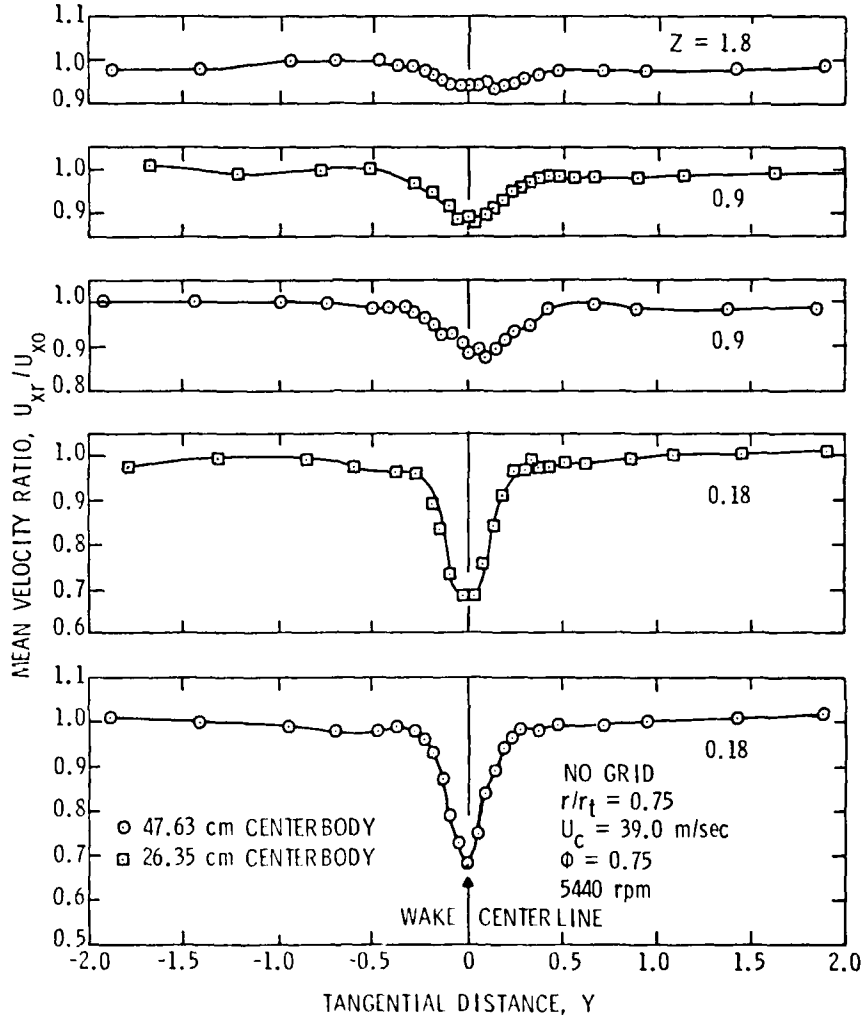

Figure IIa. Velocity Profiles of Strut Wake at r/r_t = 0.75

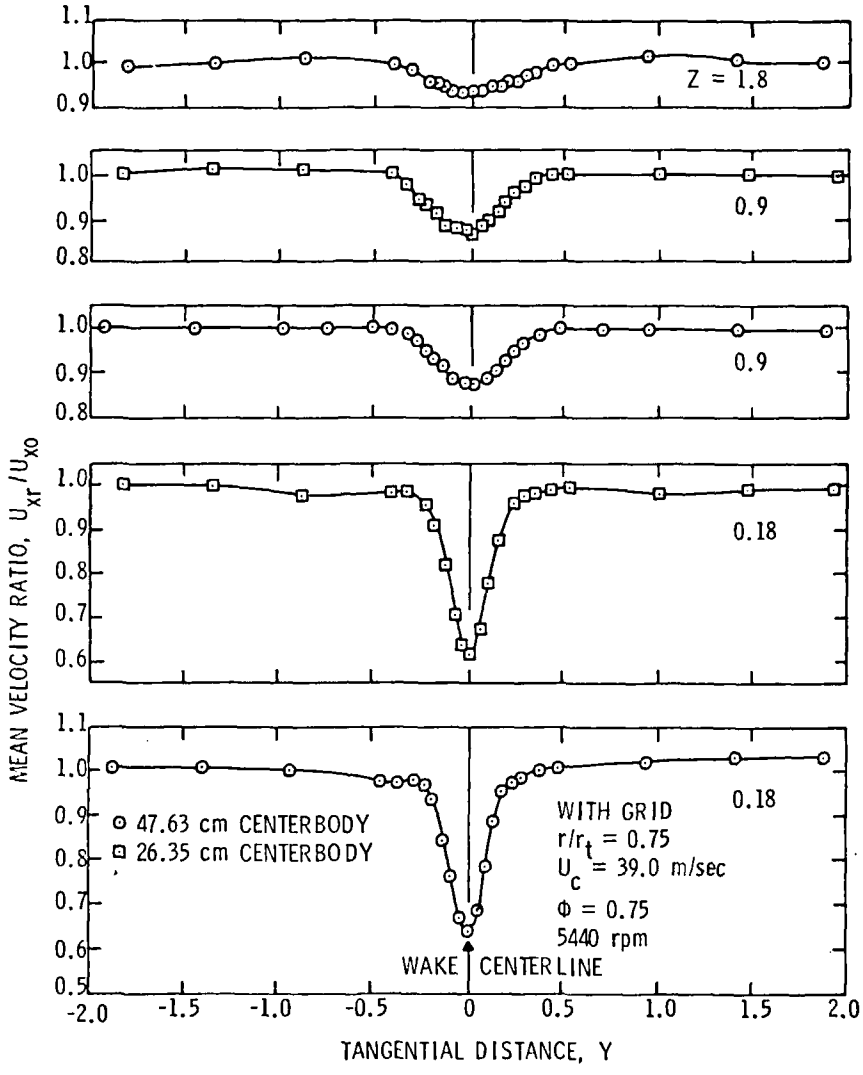

Figure 11b. Velocity Profiles of Strut Wake at $r/r_t = 0.75$

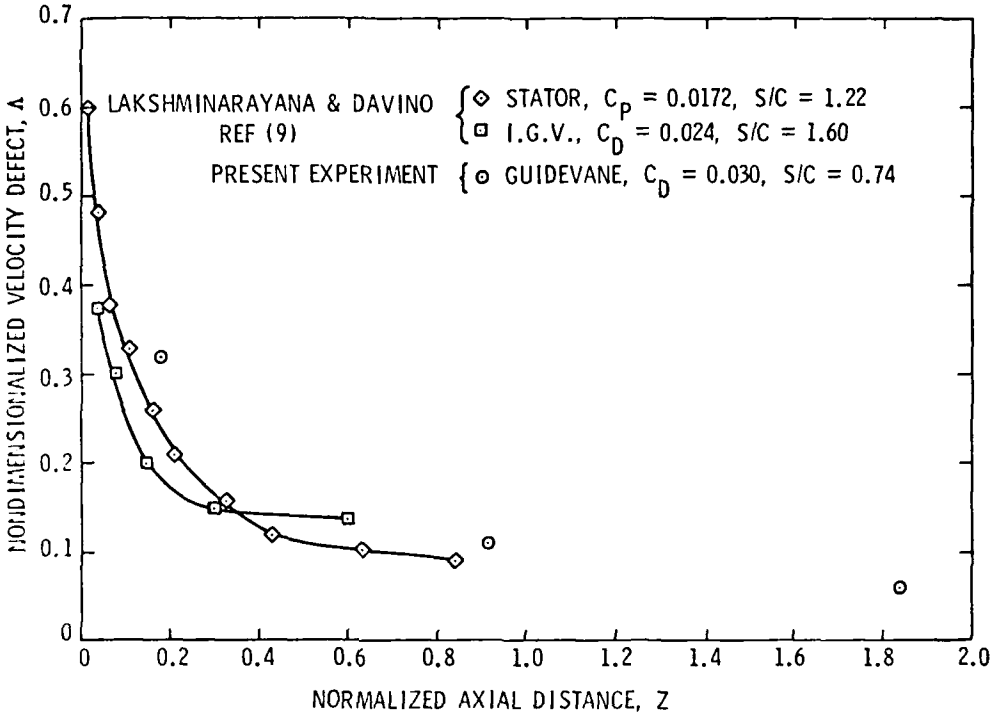

Figure 12. Decay of Velocity Defect with Axial Spacing

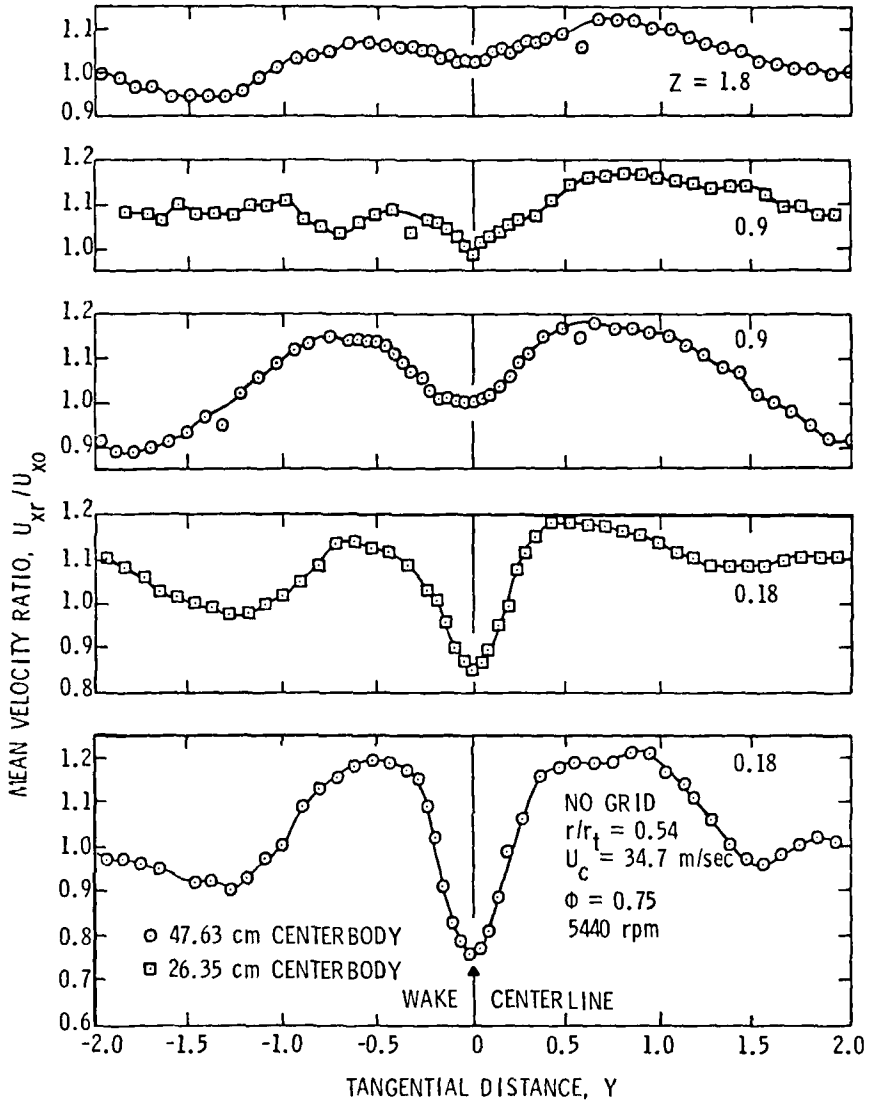

Figure 13a. Velocity Profiles of Strut Wake at $r/r_t = 0.54$

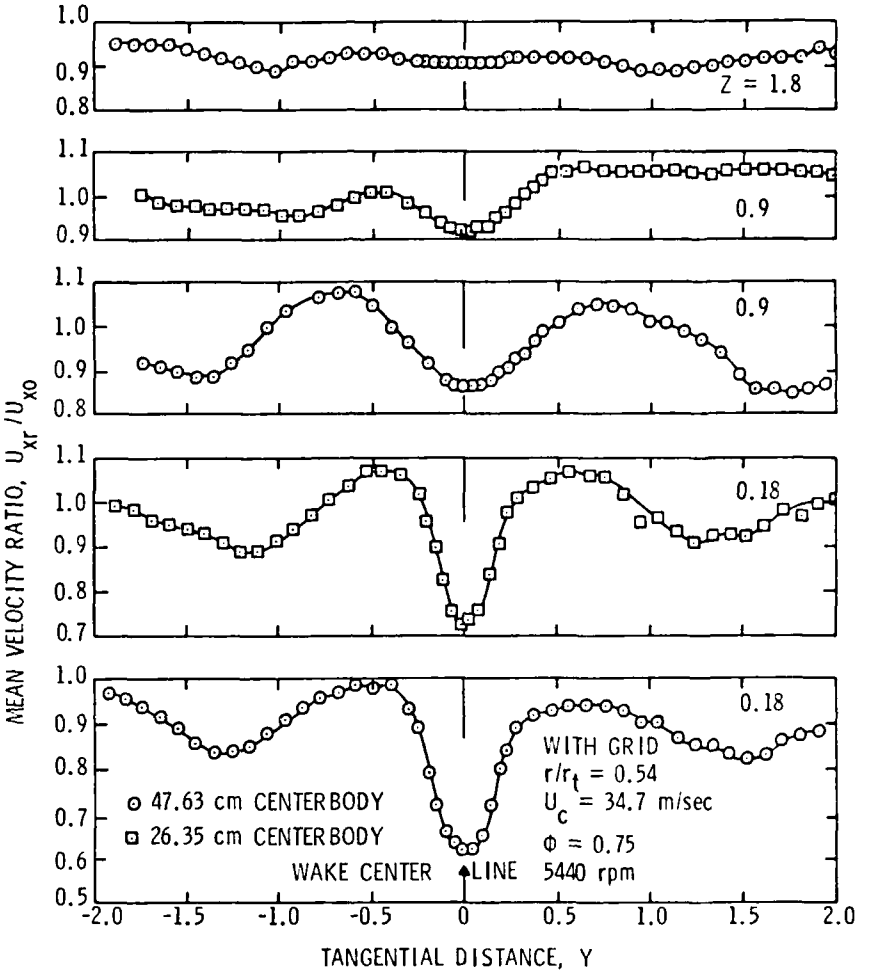

Figure 13b. Velocity Profiles of Strut Wake at $r/r_t = 0.54$

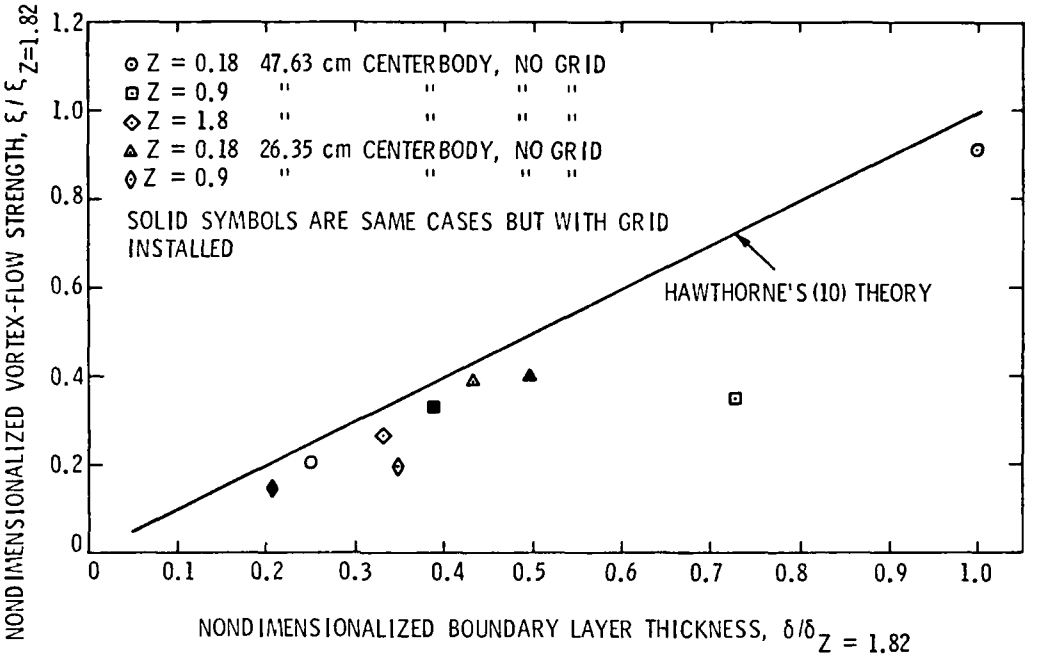

Figure 14. Comparison of Predicted Vortex Strength to Experimentally Determined Vortex Strength

25 February 1980
RT:BL:DET:cac

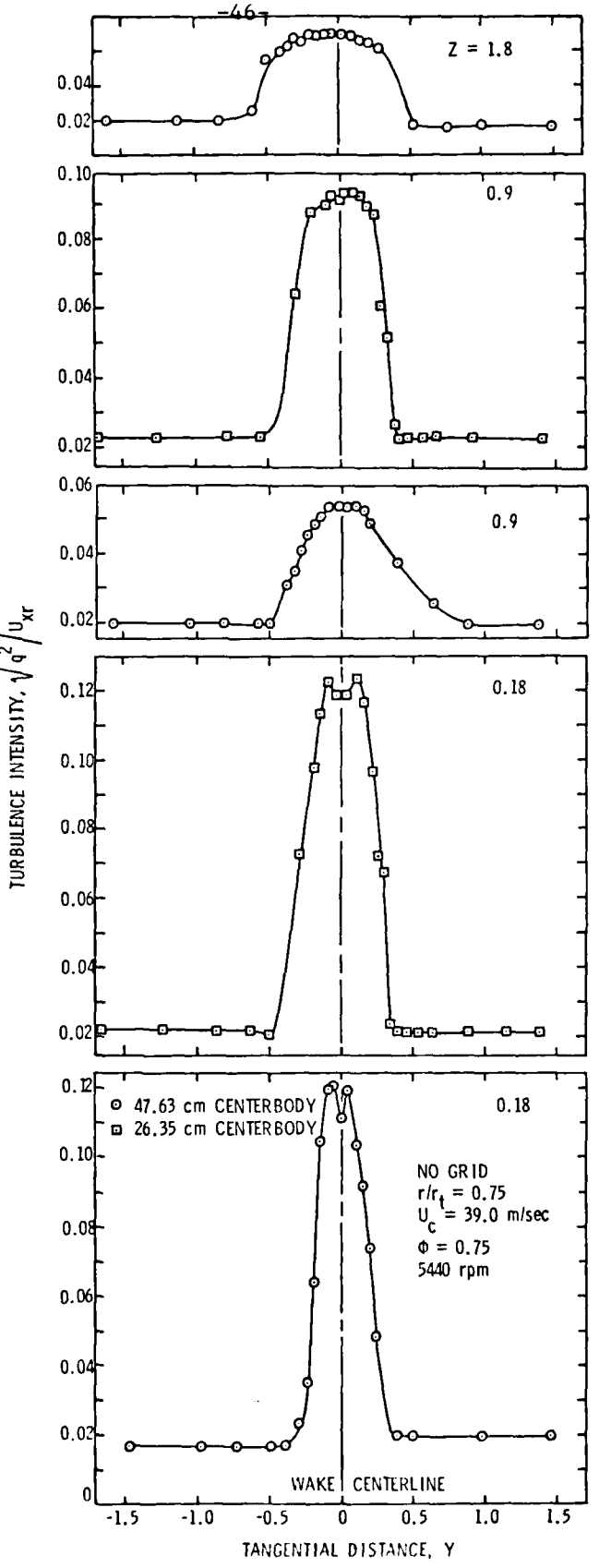

Figure 15a. Turbulence Intensity Profiles at $r/r_t = 0.75$, No Grid and Grid Cases

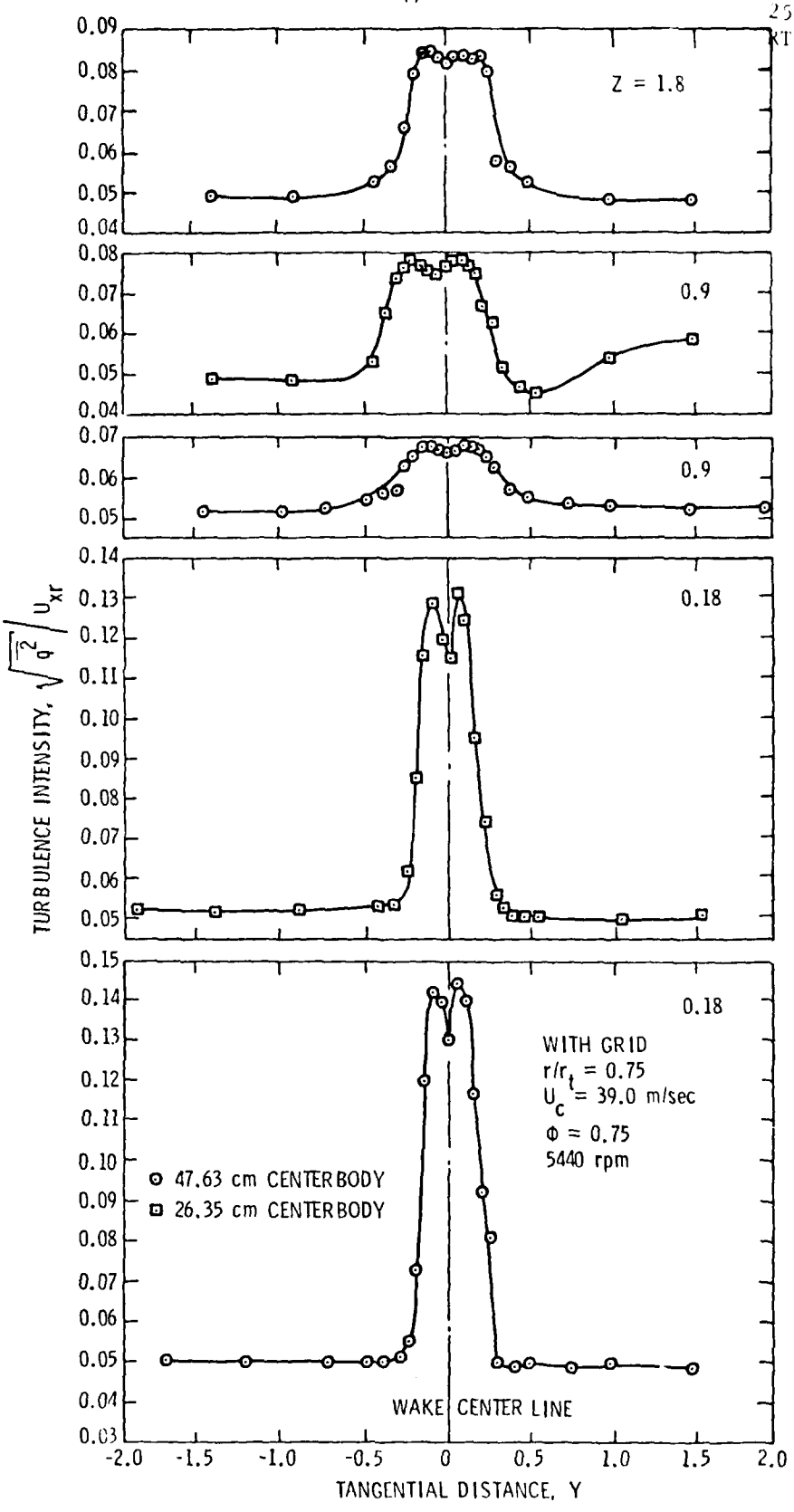

Figure 15b. Turbulence Intensity Profiles at $r/r_t = 0.75$, No Grid and Grid Cases

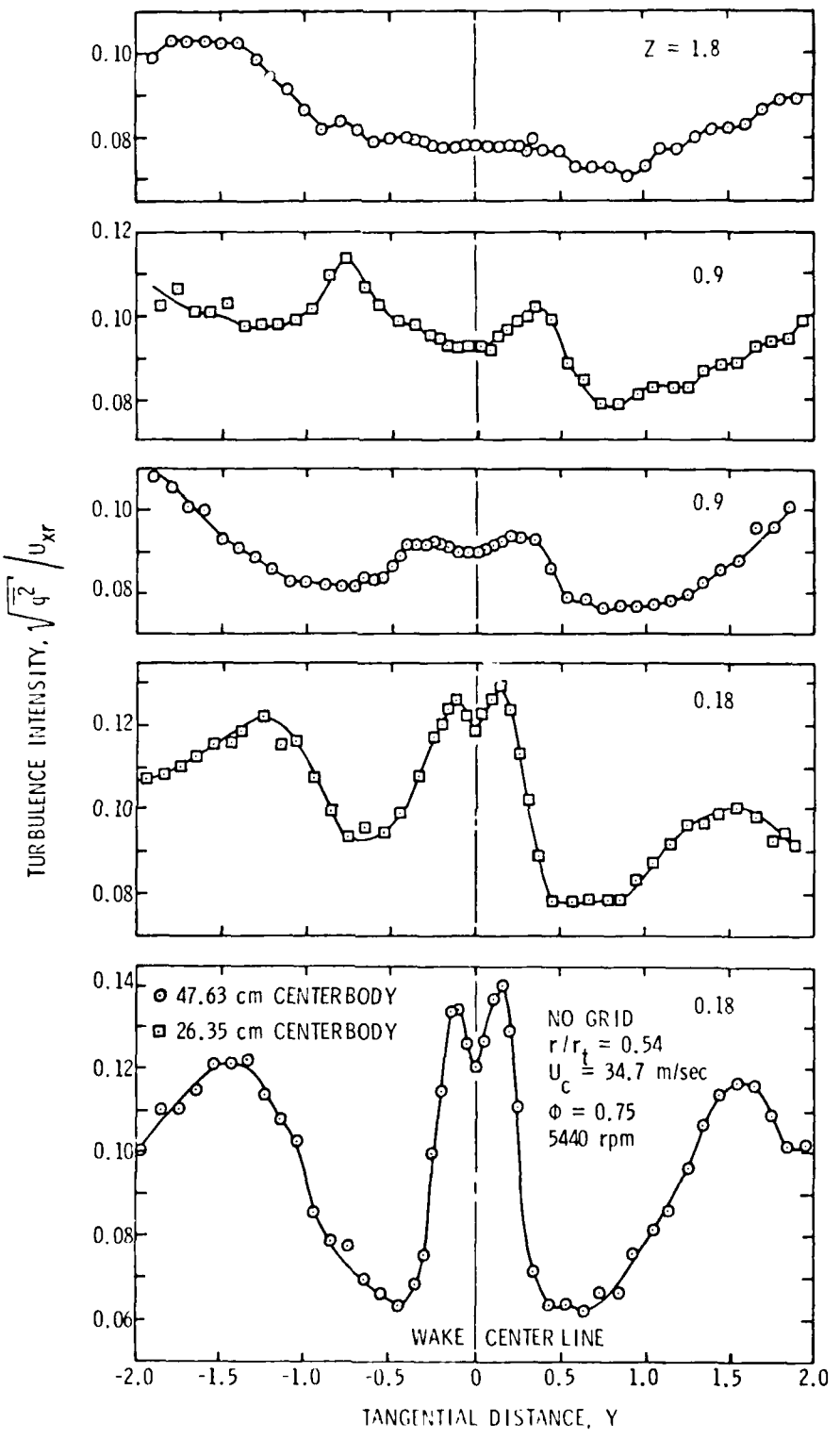

Figure 16a. Turbulence Intensity Profiles at $r/r_t = 0.54$, No Grid and Grid Cases

25 February 1980
RT:BL:DET:cac

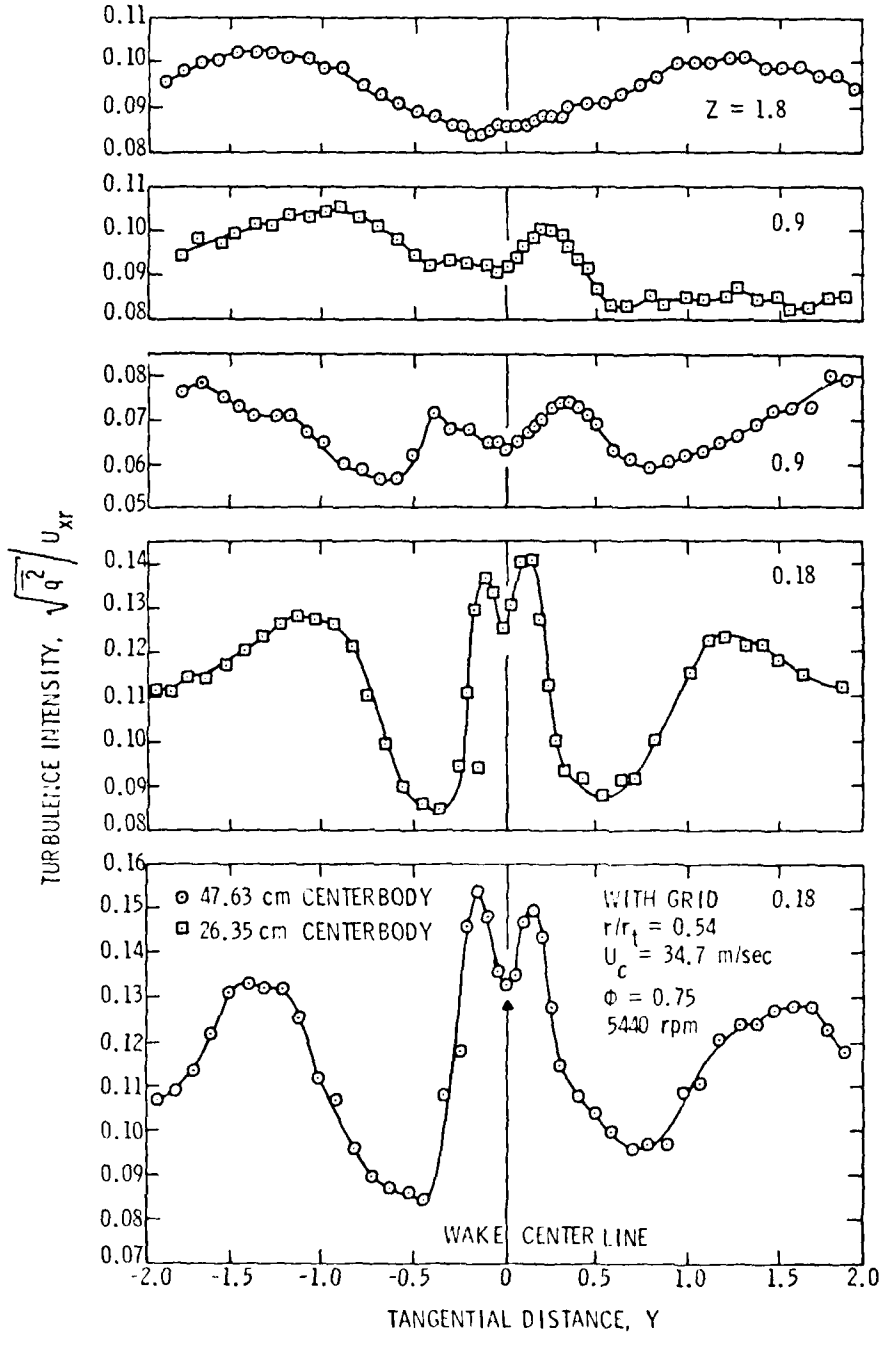

Figure 16b. Turbulence Intensity Profiles at $r/r_t = 0.54$, No Grid and Grid Cases

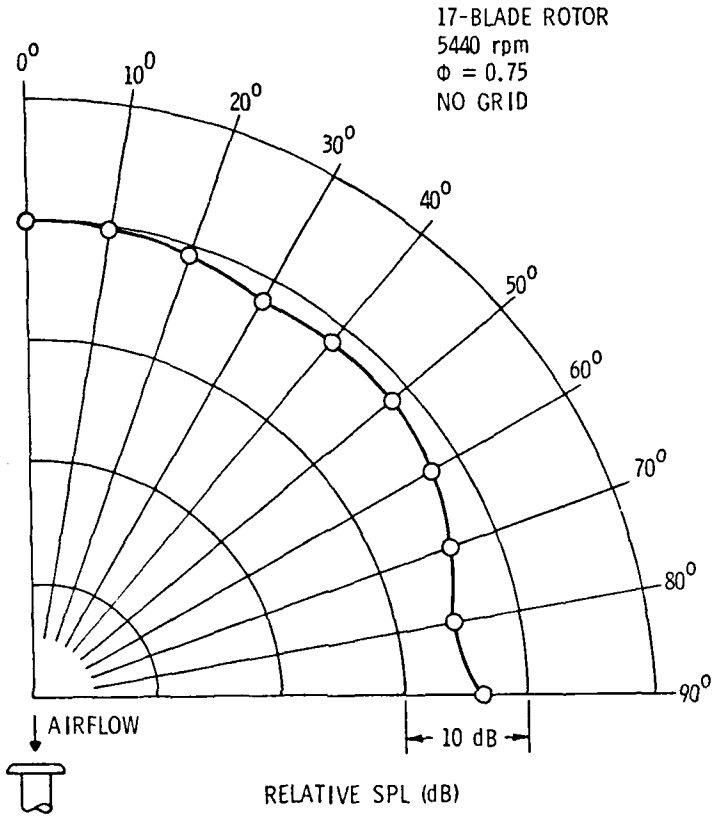

Figure 17. Typical Directivity of Far Field Sound

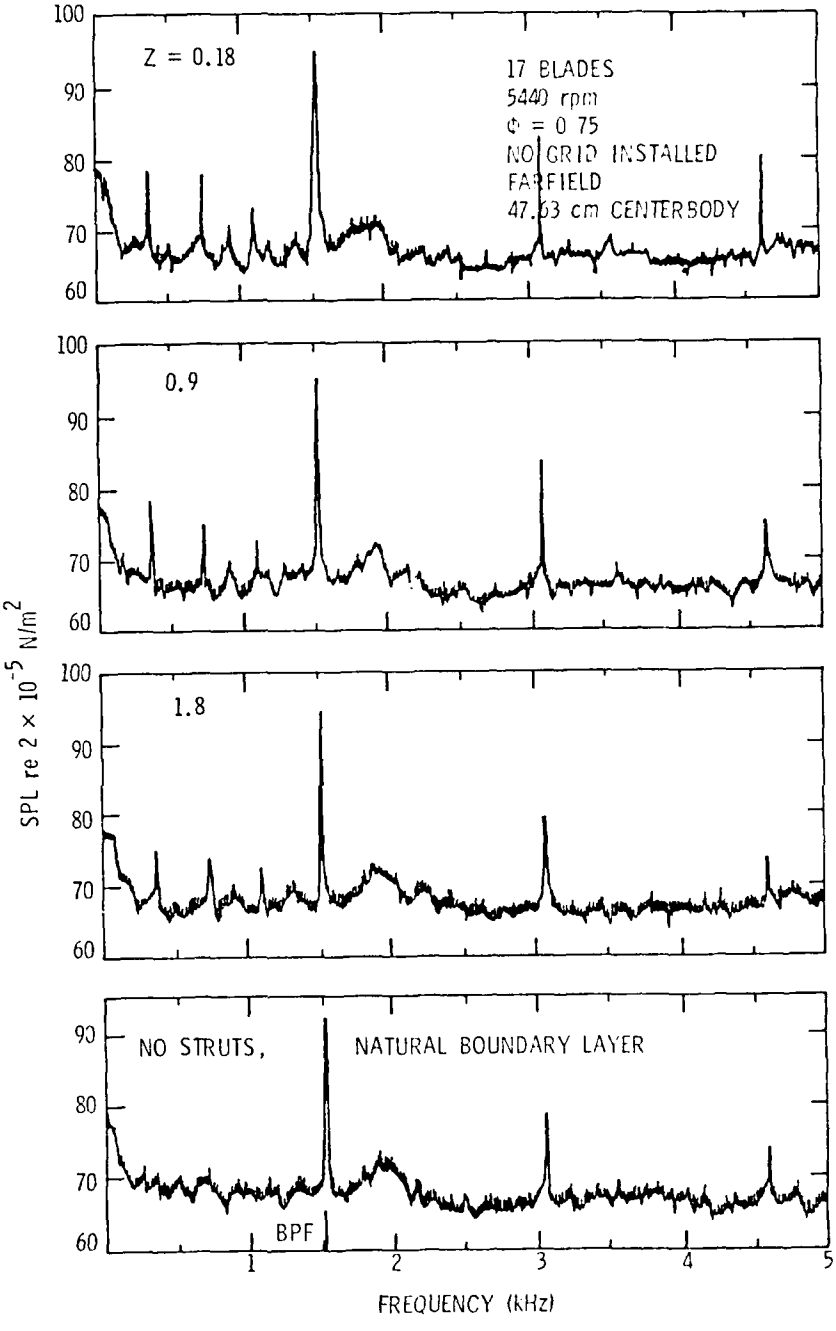

Figure 18a. Noise Spectra for 47.63 cm Centerbody, No Grid and Grid Cases

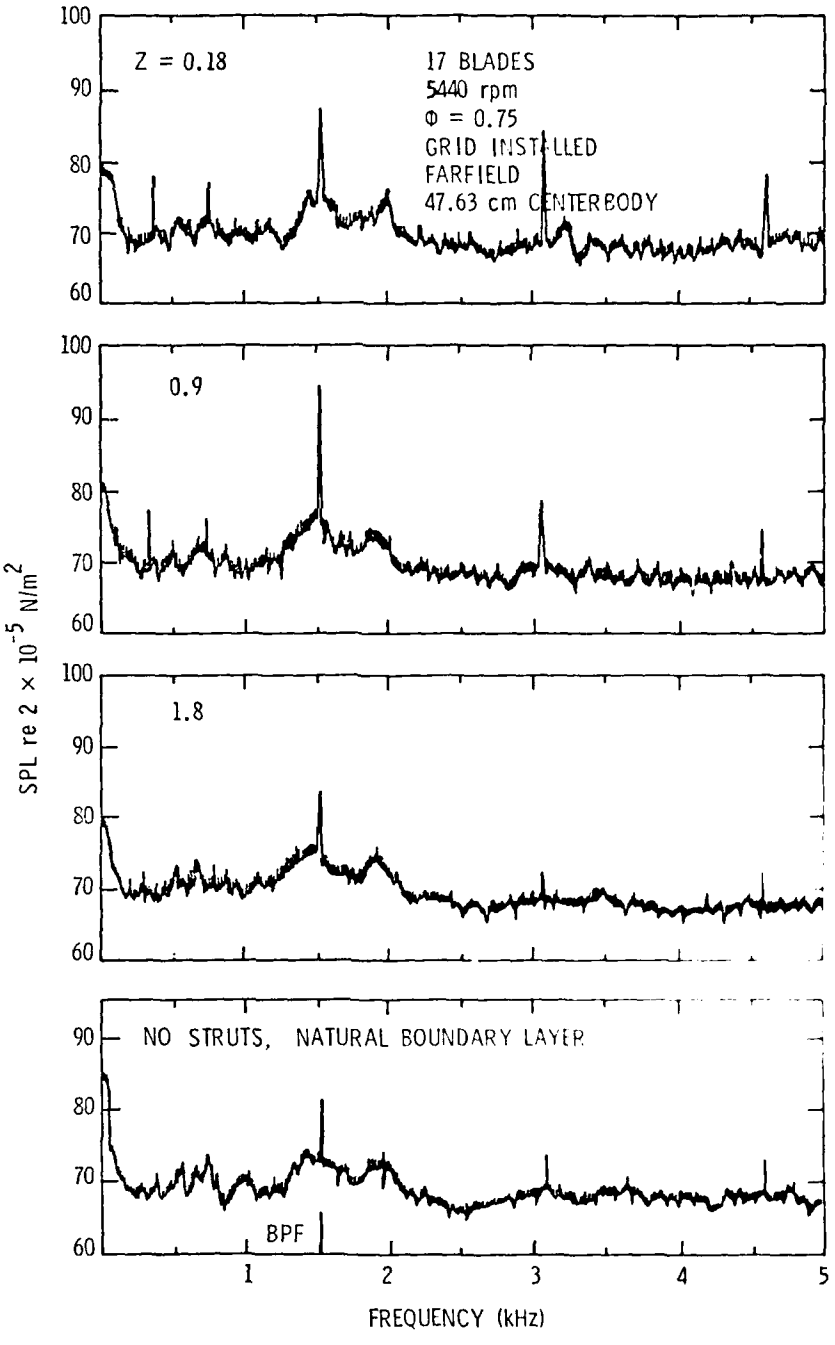

Figure 18b. Noise Spectra for 47.63 cm Centerbody, No Grid and Grid Cases

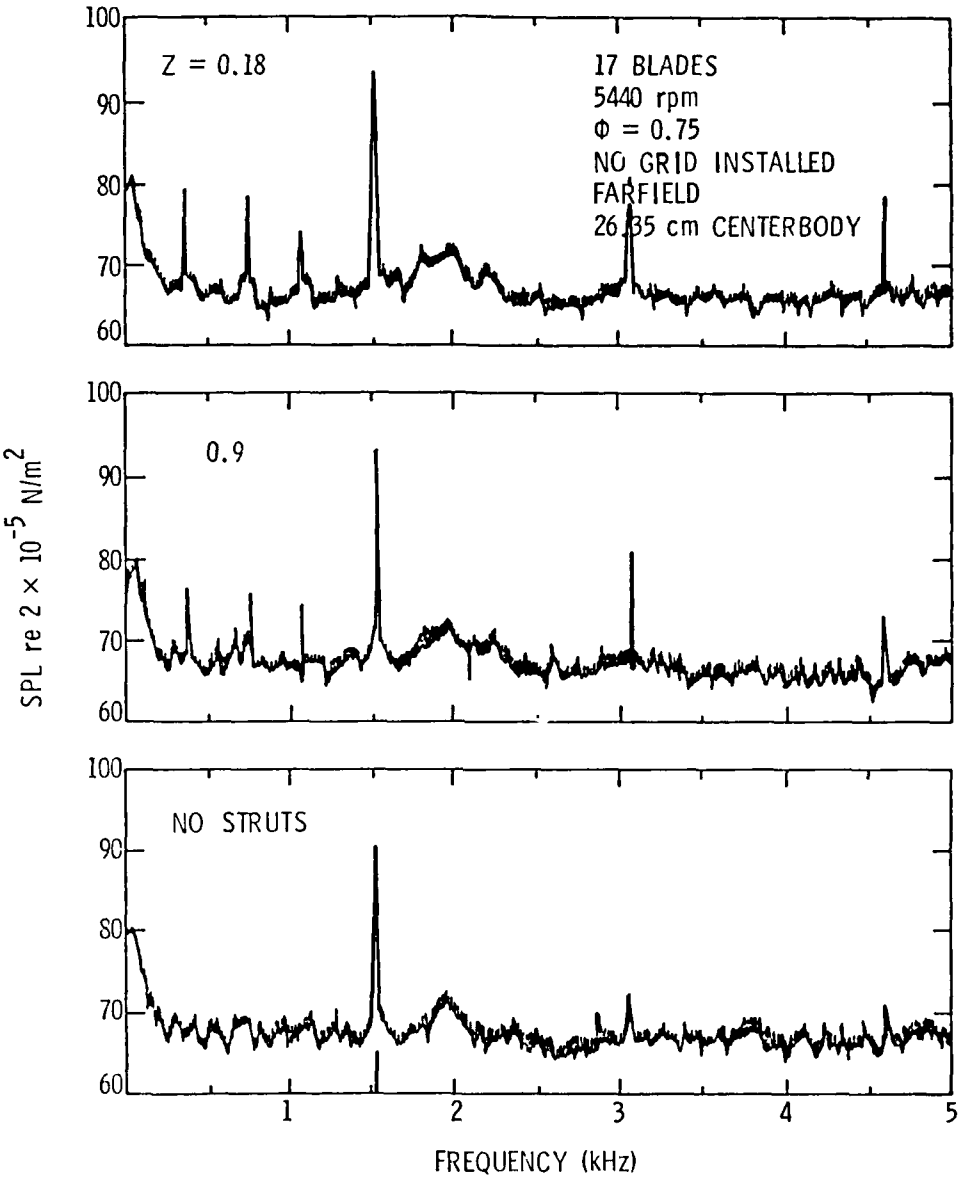

Figure 19a. Noise Spectra for 26.35 cm Centerbody, No Grid and Grid Cases

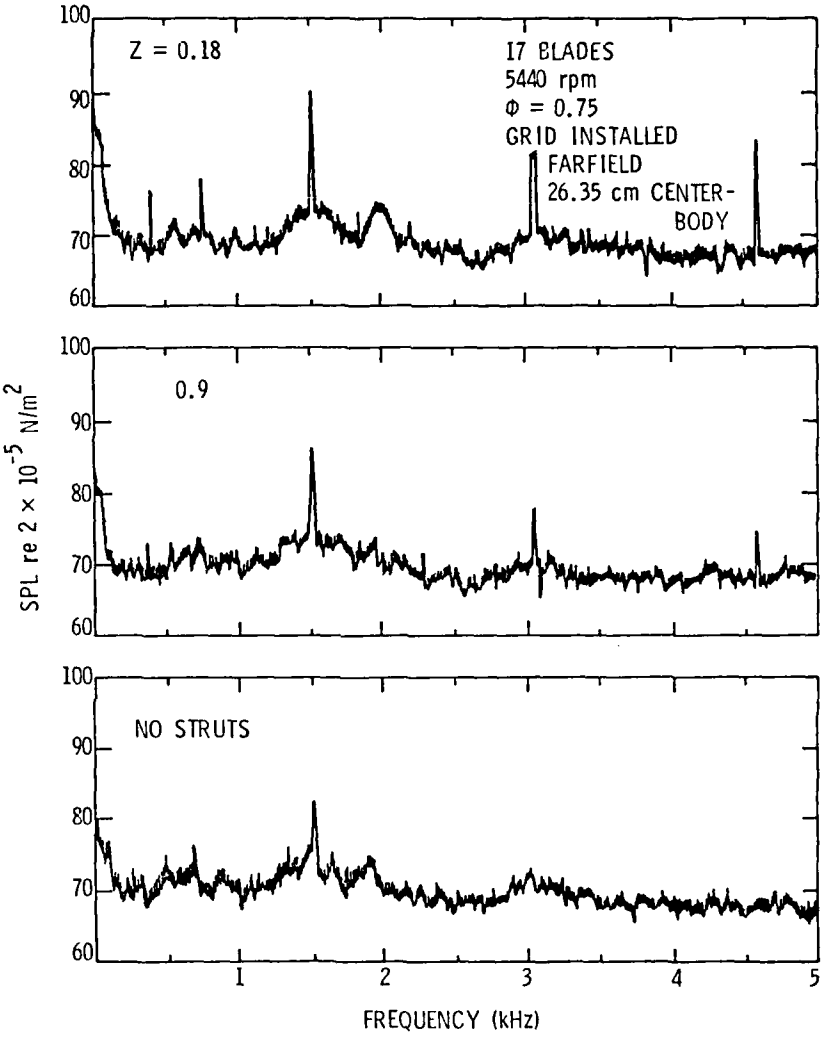

Figure 19b. Noise Spectra for 26.35 cm Centerbody, No Grid and Grid Cases

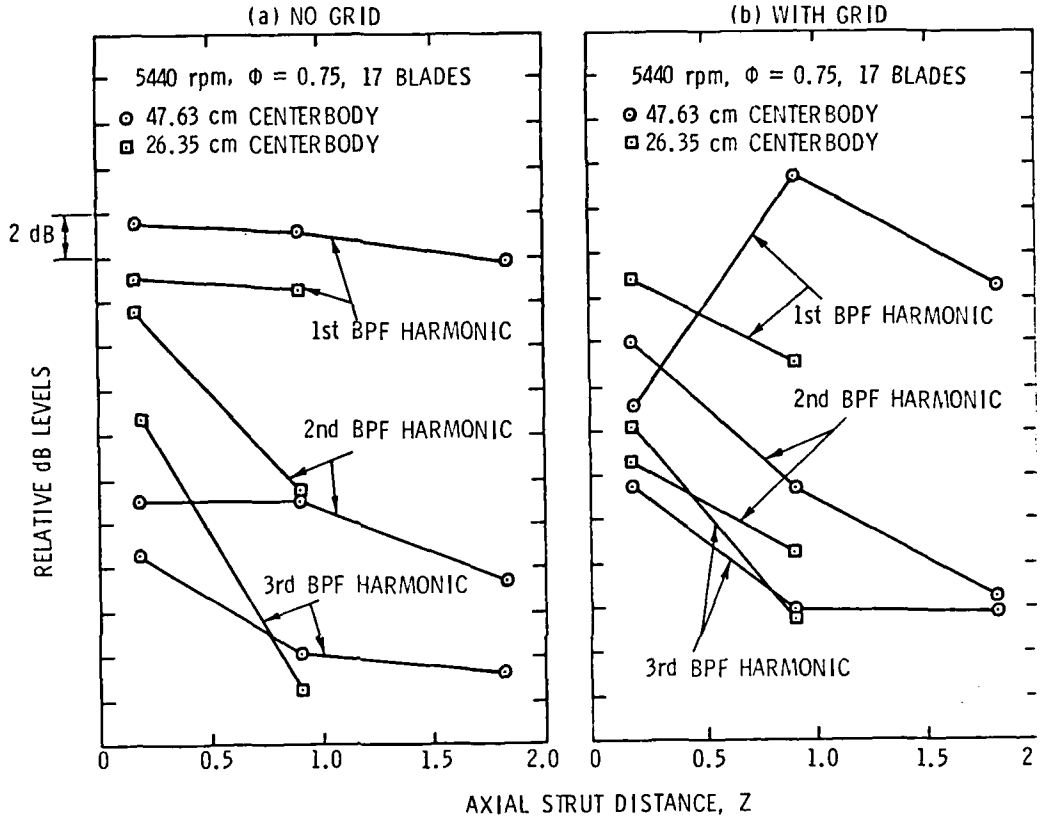

Figure 20. Variation of Blade Passing Frequencies with Strut Spacing, No Grid and Grid Cases

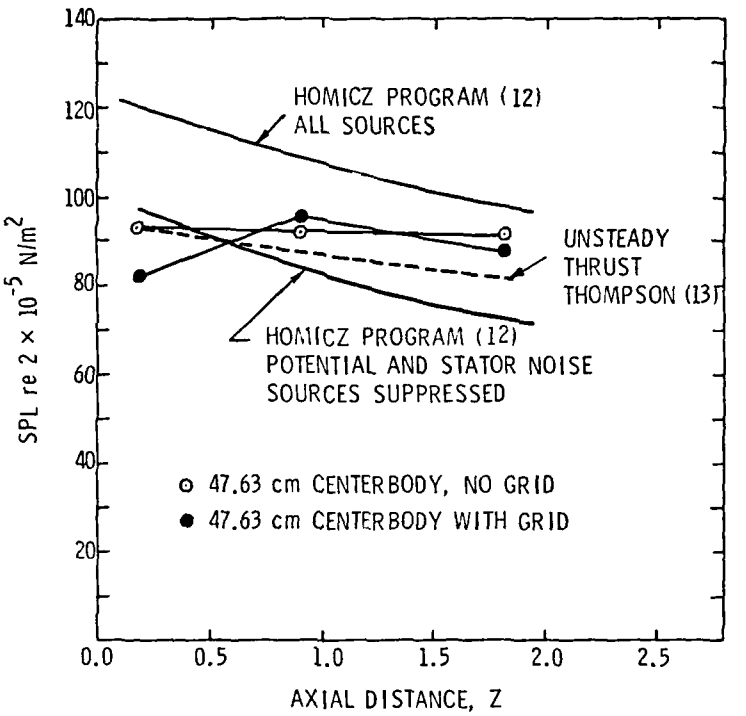

Figure 21. Comparison of Noise Predictions to Experimental Data

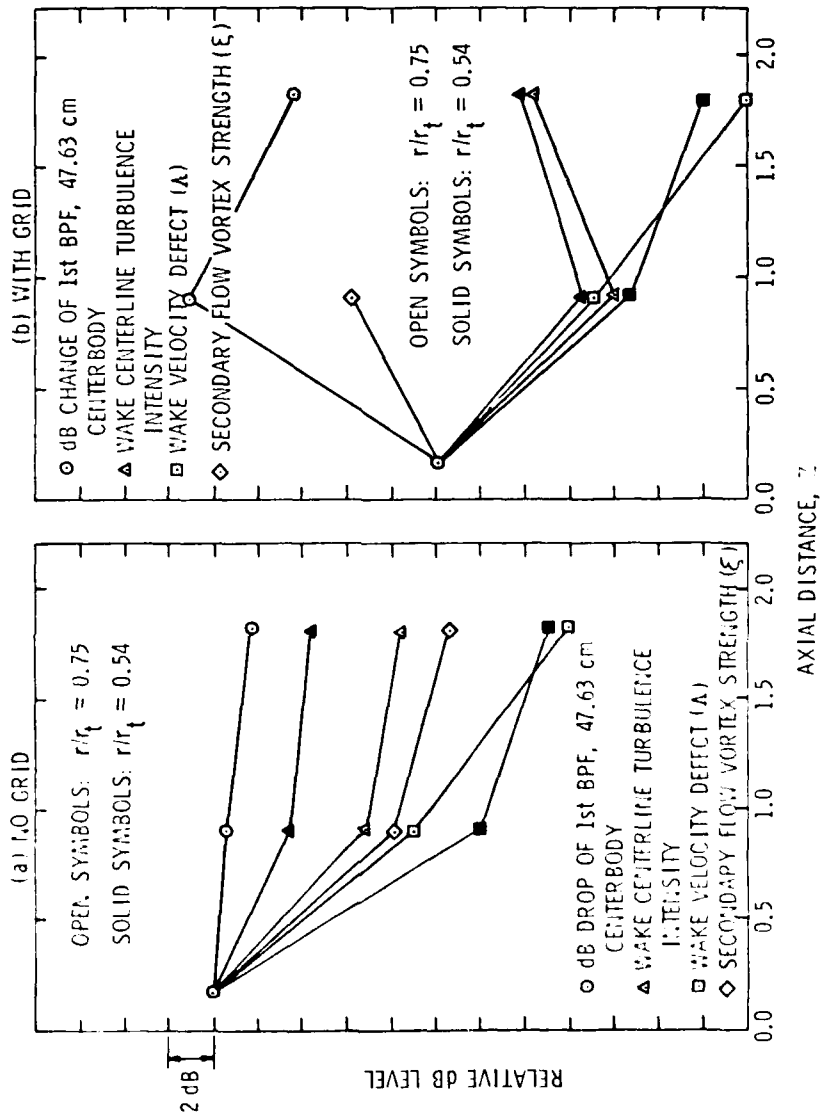

Figure 22. Comparison of Wake Parameters to the Level of the First BPF, No Grid and Grid Cases

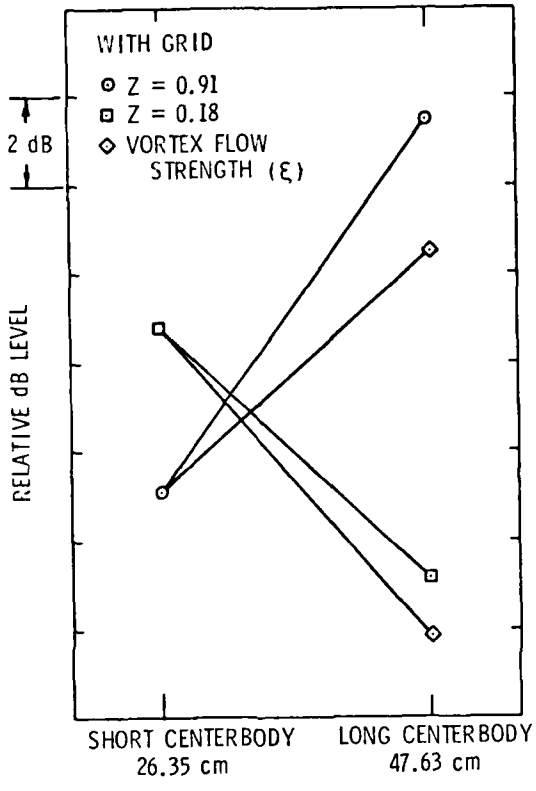

Figure 23. Comparison of Vortex Strength to the Level of the First BPF with Grid

DISTRIBUTION LIST FOR UNCLASSIFIED TM 80-20 by R. Trunzo, B. Lakshminarayana and D. E. Thompson, dated 25 February 1980.

Commander
Naval Sea Systems Command
Department of the Navy
Washington, DC 20362

Attn: S. M. Blazek
Code NSEA-05HB
(Copy No. 1)

Naval Sea Systems Command
Department of the Navy
Washington, DC 20362

Attn: H. C. Claybourne
Code NSEA-05H5
(Copy No. 2)

Naval Sea Systems Command
Department of the Navy
Washington, DC 20362

Attn: J. G. Juergens
Code NSEA-05H
(Copy No. 3)

Naval Sea Systems Command
Department of the Navy
Washington, DC 20362

Attn: T. E. Peirce
Code NSEA-63R3
(Copy No. 4)

Naval Sea Systems Command
Department of the Navy
Washington, DC 20362

Attn: A. R. Paladino
Code NSEA-05H1
(Copy No. 5)

Commading Officer
Naval Ocean Systems Center
San Diego, CA 92152

Attn: D. Nelson
Code 6342
(Copy No. 6)

Naval Ocean Systems Center
San Diego, CA 92152

Attn: M. M. Reischman
Code 2542
(Copy No. 7)

Commander
David W. Taylor Naval Ship R&D Center
Department of the Navy
Bethesda, MD 20084

Attn: W. K. Blake
Code 1942
(Copy No. 8)

David W. Taylor Naval Ship R&D Center
Department of the Navy
Bethesda, MD 20084

Attn: R. W. Brown
Code 1942
(Copy No. 9)

David W. Taylor Naval Ship R&D Center
Department of the Navy
Bethesda, MD 20084

Attn: R. A. Cumming
Code 1544
(Copy No. 10)

David W. Taylor Naval Ship R&D Center
Department of the Navy
Bethesda, MD 20084

Attn: J. H. McCarthy
Code 1552
(Copy No. 11)

David W. Taylor Naval Ship R&D Center
Department of the Navy
Bethesda, MD 20084

Attn: T. C. Mathews
Code 1942
(Copy No. 12)

David W. Taylor Naval Ship R&D Center
Department of the Navy
Bethesda, MD 20084

Attn: W. B. Morgan
Code 1942
(Copy No. 13)

David W. Taylor Naval Ship R&D Center
Department of the Navy
Bethesda, MD 20084

Attn: M. M. Sevik
Code 19
(Copy No. 14)

DISTRIBUTION LIST FOR UNCLASSIFIED TM 80-20 by R. Trunzo, B. Lakshminarayana and D. E. Thompson, dated 25 February 1980

David W. Taylor Naval Ship R&D Center
Department of the Navy
Bethesda, MD 20084
Attn: V. J. Monacella, Code 1505
(Copies 15 to and including No. 39)

National Bureau of Standards
Aerodynamics Section
Washington, DC 20234

Attn: P. S. Klebanoff
(Copy No. 40)

Dr. Henry T. Falvey
Engineering & Research Center
Bureau of Reclamation
U.S. Dept. of the Interior
Room 28, Bldg. 56
P.O. Box 25007
Denver Federal Center
Denver, CO 80225
(Copy No. 41)

Dr. Peter van Oossanen
Netherlands Ship Model Basin
Haagsteeg 2
P.O. Box 28
67 AA Wageningen
The Netherlands
(Copy No. 42)

Dr. rer. nat. Horst Merbt
Forschungsbeauftragter fur Hydroakustik
8012 Ottobrunn B. Munchen
Waldparkstr. 41
Munich
Germany
(Copy No. 43)

Ir. A. M. Stuurman
Ministerie van Defensie (Marine)
Hoofdasdeling Material
Porenstratt 172
Koningin Marialaan 17
Den Hague
The Netherlands
(Copy No. 44)

Dr. Ir. A. De Bruijn
Technisch Physische Dienst TNO-TH
Stieltjesweg 1
Postbuf 155
Delft
The Netherlands
(Copy No. 45)

Dr. John Foxwell
Admiralty Research Laboratory
Teddington, Middlesex
England
(Copy No. 46)

Dr. Allen Moore
Admiralty Research Laboratory
Teddington, Middlesex
England
(Copy No. 47)

Professor J. P. Gostelow
School of Mechanical Engineering
NSW Institute of Technology
Broadway
Sidney
Australia
(Copy No. 48)

Bolt, Beranek and Newman
50 Moulton Street
Cambridge, MA 20136

Attn: Dr. N. A. Brown
(Copy No. 49)

Bolt, Beranek and Newman
50 Moulton Street
Cambridge, MA 20136

Attn: D. Chase
(Copy No. 50)

Bolt, Beranek and Newman
50 Moulton Street
Cambridge, MA 20136

Attn: K. L. Chandiramani
(Copy No. 51)

Mr. E. M. Greitzer
MS-16 United Technologies
Research Center
Silver Lan
E. Hartford, CT 06118
(Copy No. 52)

Defense Documentation Center
5010 Duke Street
Cameron Station
Alexandria, VA 22314
(Copies 53 to and including 64)

DISTRIBUTION LIST FOR UNCLASSIFIED TM 80-20 by R. Trunzo, B. Lakshminarayana and D. E. Thompson, dated 25 February 1980

The Pennsylvania State University
Applied Research Laboratory
Post Office Box 30
State College, PA 16801

Attn: B. R. Parkin
(Copy No. 65)

Applied Research Laboratory
Attn: R. E. Henderson
(Copy No. 66)

Applied Research Laboratory
Attn: G. C. Lauchle
(Copy No. 67)

Applied Research Laboratory
Attn: F. S. Archibald
(Copy No. 68)

Applied Research Laboratory
Attn: B. E. Robbins
(Copy No. 69)

Applied Research Laboratory
Attn: GTWT Files
(Copy No. 70)

Applied Research Laboratories
Attn: D. E. Thompson
(Copy No. 71)

The Pennsylvania State Univeristy
Aerospace Engineering Department
Attn: B. Lakshminarayana
(Copy No. 72)

Raymond Trunzo
Rockwell International Space Division
12214 Lakewood Blvd.
Downey, CA 90241
(Copy No. 73)

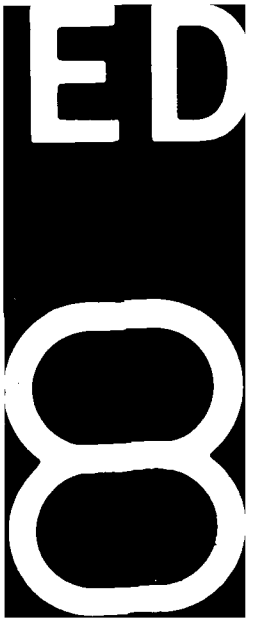
ED
8